NASA Technical Paper 1578

Analyses of Surface Cracks in Finite Plates Under Tension or Bending Loads

J. C. Newman, Jr., and I. S. Raju

DECEMBER 1979

NASA

NASA Technical Paper 1578

Analyses of Surface Cracks in Finite Plates Under Tension or Bending Loads

J. C. Newman, Jr.
Langley Research Center
Hampton, Virginia

I. S. Raju
The George Washington University
Joint Institute for Advancement of Flight Sciences
Langley Research Center
Hampton, Virginia

National Aeronautics
and Space Administration

**Scientific and Technical
Information Branch**

1979

SUMMARY

This paper presents stress-intensity factors calculated with a three-dimensional, finite-element analysis for shallow and deep semielliptical surface cracks in finite elastic isotropic plates subjected to tension or bending loads. A wide range of configuration parameters was investigated. The ratio of crack depth to plate thickness ranged from 0.2 to 0.8 and the ratio of crack depth to crack length ranged from 0.2 to 2.0. The effects of plate width on stress-intensity variations along the crack front were also investigated.

A wide-range equation for stress-intensity factors along the crack front as a function of crack depth, crack length, plate thickness, and plate width was developed for tension and bending loads. The equation was used to predict patterns of surface-crack growth under tension or bending fatigue loads. A modified form of the equation was also used to correlate surface-crack fracture data for a brittle epoxy material within ±10 percent for a wide range of crack shapes and crack sizes.

INTRODUCTION

Surface cracks are common flaws in many structural components. Accurate stress analyses of these surface-cracked components are needed for reliable prediction of their crack-growth rates and fracture strengths. However, because of the complexities of such problems, exact solutions are not available. Investigators have used experimental or approximate analytical methods to obtain stress-intensity factors for surface cracks under tension or bending loads. For a semielliptical surface crack in a plate of finite thickness (fig. 1), Smith and Alavi (ref. 1), Smith and Sorensen (ref. 2), and Kobayashi et al. (ref. 3) used the alternating method to obtain the stress-intensity factor variations along the crack front for various crack shapes. Kathiresan (ref. 4) used the finite-element method to obtain the same information. However, there is considerable disagreement in the values from these solutions.

This paper presents stress-intensity factors calculated from a three-dimensional, finite-element analysis for shallow and deep semielliptical surface cracks in finite elastic plates subjected to tension or bending loads. Details of the finite-element analysis are discussed in references 5 and 6, in which limited stress-intensity factor results for tension loads are also presented. The present study covers a wide range of configuration parameters. The ratio of crack depth to plate thickness ranged from 0.2 to 0.8; the ratio of crack depth to crack length ranged from 0.2 to 2.0. The effect of plate width on stress-intensity factor variations along the crack front was also investigated. The stress-intensity factors were calculated by using a nodal-force method (refs. 6 and 7). This method was preferred to the commonly used crack-opening-displacement method (ref. 8), which requires a prior assumption of either plane stress or plane strain. This introduces a potential source of inaccuracy. The nodal-force method requires no such assumption.

A wide-range equation for the stress-intensity factors along the crack front as a function of crack depth, crack length, plate thickness, and plate width was also developed for tension and bending loads. In appendix A, the equation is used to predict surface-crack-growth patterns under tension or bending fatigue loads. These predicted patterns are also compared with measurements reported in the literature for steel, titanium alloy, and aluminum alloy materials. In appendix B, a modified form of the stress-intensity equation is also used to correlate surface-crack fracture data reported in the literature for a brittle epoxy material.

SYMBOLS

a	depth of surface crack, mm
b	half-width of cracked plate, mm
C_A, C_B	crack-growth coefficients (see eqs. (A1) and (A2))
c	half-length of surface crack, mm
F	stress-intensity boundary-correction factor
h	half-length of cracked plate, mm
K_I	mode I stress-intensity factor, $kN/m^{3/2}$
K_{cr}	elastic fracture toughness, $kN/m^{3/2}$
M	applied bending moment, N-m
M_e	elastic magnification factor (see eqs. (B1) and (B2))
N	number of cycles
n	exponent in equation for crack-growth rate
Q	shape factor for elliptical crack
S_b	remote bending stress on outer fiber, $3M/bt^2$, Pa
S_t	remote uniform-tension stress, Pa
t	plate thickness, mm
X,Y,Z	Cartesian coordinate system
ΔK	stress-intensity factor range, $kN/m^{3/2}$
ν	Poisson's ratio
ϕ	parametric angle of the ellipse, deg

THREE-DIMENSIONAL, FINITE-ELEMENT ANALYSIS

A three-dimensional, finite-element analysis was used to calculate the mode I stress-intensity factor variations along the crack front for a surface crack in a finite plate. The plate was subjected to remote tension or bending loads and is shown in figure 1.

Figure 2(a) shows a typical finite-element model of a plate containing a surface crack. Symmetry conditions on the $x = 0$ and the $y = 0$ planes allow attention to be restricted to one-quarter of the plate. Two types of elements, isoparametric and singular, were used in combination to model the surface-cracked plate. The arrangement of elements on the crack plane ($y = 0$) is shown in figure 2(b). The isoparametric elements (linear strain, denoted as I) were used everywhere except near the crack front. Around the crack front, eight singularity elements (denoted as S) in the shape of pentahedrons were arranged as shown in figure 2(c). The assumed displacement distribution of the singularity elements had square-root terms, and therefore produced a singular stress field at the crack front. Details of the formulation of these types of elements are given in references 7 and 8 and are not repeated here. The particular finite-element models used were established with the help of a convergence study performed in references 5 and 6. The models had 4300 to 4800 degrees of freedom.

Loading

Two types of loads were applied to the finite-element models of the surface-cracked plate: remote uniform tension and remote bending. The remote uniform-tension stress is S_t in figure 3(a); the remote outer-fiber bending stress S_b in figure 3(b) is calculated from the applied bending moment M.

Stress-Intensity Factor

Only loads which cause mode I deformations were considered. The mode I stress-intensity factor K_I for any point along the surface-crack front was taken to be

$$K_I = S_i\sqrt{\pi \frac{a}{Q}}\, F_i\left(\frac{a}{t}, \frac{a}{c}, \frac{c}{b}, \phi\right) \tag{1}$$

where the subscript i denotes either tension load ($i = t$) or bending load ($i = b$), and Q, the shape factor for an ellipse, is given by the square of the complete elliptic integral of the second kind (ref. 9). The half-length of the plate h was chosen large enough to have a negligible effect on stress intensity ($h/c = 5$). Values for F, the boundary-correction factor, were calculated along the crack front for various combinations of parameters with these ranges: $0.2 \leqq a/c \leqq 2.0$, $0.2 \leqq a/t \leqq 0.8$, and $0.2 \leqq c/b \leqq 0.8$.

The stress-intensity factors were obtained by use of a nodal-force method, the details of which are given in references 6 and 7. In this method, the nodal forces normal to the crack plane and ahead of the crack front are used to evaluate the stress-intensity factor.

RESULTS AND DISCUSSION

In the following sections, stress-intensity factors for semielliptical surface cracks in plates subjected to tension or bending loads are presented. The effects of crack shape (a/c), crack size (a/t), and plate width (c/b) are investigated. The stress-intensity factors are compared with other values from the literature. Also, a wide-range equation for stress-intensity factors as a function of the parametric angle, crack shape, crack size, and plate width is developed herein from the present results.

Tension

Effects of a/c and a/t.- Figure 4 shows the normalized stress-intensity factors as functions of the parametric angle ϕ and the ratio of crack depth to plate thickness a/t for a semielliptical surface crack ($0.2 \leq a/c \leq 2.0$) in a plate under uniform-tension load. The c/b ratio was taken to be less than or equal to 0.2, so that plate width would have a negligible effect on stress intensity (less than 1 percent). For every a/c ratio and parametric angle considered, larger values of a/t gave larger normalized stress-intensity factors. For low a/c ratios, the maximum normalized stress-intensity factor occurs at the point of maximum depth ($\phi = \pi/2$), whereas for high a/c ratios the maximum factor occurs at the intersection of the crack with the front surface ($\phi = 0$). The normalized stress-intensity factors for tension are given in table I.

Effects of c/b.- The normalized stress-intensity factors for a semielliptical surface crack in a finite-width plate are given in table II for $a/c = 0.2$ or 1.0 and ϕ from 0 to $\pi/2$ for various values of c/b and a/t.

In figures 5(a) and 5(b), the normalized stress-intensity factors for semicircular and semielliptical surface cracks, respectively, are plotted as functions of ϕ for $a/t = 0.8$ and for c/b from 0.2 to 0.8. For the semicircular crack ($a/c = 1.0$), the stress-intensity factors, which are maximum at $\phi = 0$, are higher for larger c/b ratios. The dashed lines in figure 5(a) show the corresponding stress-intensity factors for a through crack of length 2c. The values for a surface crack at $\phi = 0$ are about 10 percent lower than the values for a through crack of the same length.

In figure 5(b), the stress-intensity factors for the semielliptical crack ($a/c = 0.2$) are maximum at $\phi = \pi/2$. Again, larger c/b ratios gave higher stress-intensity factors.

Comparisons with other solutions.- Figures 6(a) and 6(b) show, respectively, normalized stress-intensity factors obtained by several investigators for semicircular and semielliptical surface cracks in a finite-thickness plate. The results in figure 6(a) are for $a/c = 1.0$ and $a/t = 0.8$. The present results (solid symbols) are 10 to 15 percent higher than the results of Smith and Alavi (ref. 1) and Kobayashi (ref. 3) for low values of the parametric angle. The results of Kathiresan (ref. 4) are fairly close to the present results. All solutions agree well near $\phi = \pi/2$.

Figure 6(b) shows the results for a semielliptical surface crack with $a/c = 0.2$ and $a/t = 0.8$. The solutions of Smith and Sorensen (ref. 2), Kobayashi (ref. 3), and Kathiresan (ref. 4) disagree by 50 to 100 percent. Also, these solutions are considerably below the present results. The results from reference 2 are generally closer to the present results, although 10 to 25 percent lower.

Bending

Effects of a/c and a/t.- Figure 7 shows the normalized stress-intensity factors as functions of the parametric angle and a/t ratios for semielliptical surface cracks ($0.2 \leq a/c \leq 2.0$) subjected to bending loads. (See fig. 3(b).) Again, the c/b ratio was less than or equal to 0.2. For all a/c ratios and high a/t ratios, the maximum normalized stress-intensity factor occurs at the front surface ($\phi = 0$). For the lowest a/t ratio considered (0.2), the stress-intensity factor variations along the crack front are similar to the tension case. Table I gives the normalized stress-intensity factors for these crack configurations.

Effects of c/b.- The normalized stress-intensity factors for a semielliptical surface crack ($a/c = 0.2$ or 1.0) are given in table II for various values of c/b, a/t, and ϕ.

Figures 8(a) and 8(b) show, respectively, the stress-intensity factors for semicircular ($a/c = 1.0$) and semielliptical ($a/c = 0.2$) surface cracks as functions of ϕ for $a/t = 0.8$ and c/b from 0.2 to 0.8. For both crack shapes, the stress-intensity factor is maximum at the front surface ($\phi = 0$). The stress-intensity factors are higher for larger c/b ratios.

Comparisons with other solutions.- Figures 9(a) and 9(b) show stress-intensity factors obtained by investigators for semicircular surface cracks in a wide plate under bending loads with $a/t = 0.6$ and 0.8. For $a/t = 0.6$ and $\phi < \pi/4$ (fig. 9(a)), the present results fall between those of Kobayashi (ref. 3) and Kathiresan (ref. 4). For $\phi > \pi/4$, the results are in close agreement.

The results in figure 9(b) are for a deeper semicircular surface crack ($a/t = 0.8$) than that shown in figure 9(a). Here the present results are

generally higher by about 10 percent than Kathiresan's and Kobayashi's results for $\phi < \pi/4$.

Stress-Intensity Factor Equation for the Surface Crack

For ease of computation, a wide-range equation for the stress-intensity factor of a surface crack in a finite plate subjected to tension and bending loads has been fitted to the present finite-element results for a/c from 0.2 to 1.0. To account for the limiting behavior as a/c approaches zero, the results of Gross and Srawley (ref. 10) for a single-edge crack have also been used. The stress-intensity factor equation for combined tension and bending loads is

$$K_I = (S_t + HS_b)\sqrt{\pi \frac{a}{Q}}\, F \tag{2}$$

for $0 < a/c \leqq 1.0$, $0 \leqq a/t < 1.0$, $c/b < 0.5$, and $0 \leqq \phi \leqq \pi$. A useful approximation for Q, developed by Rawe and used in reference 11, is

$$Q = 1 + 1.464\left(\frac{a}{c}\right)^{1.65} \qquad \left(\frac{a}{c} \leqq 1\right) \tag{3}$$

The functions F and H are defined so that the boundary-correction factor for tension is equal to F and the boundary-correction factor for bending is equal to the product of H and F. The function F was obtained from a systematic curve-fitting procedure by using double-series polynomials in terms of a/c, a/t, and angular functions of ϕ. The choice of functions was based on engineering judgment. The function F was taken to be

$$F = \left[M_1 + M_2\left(\frac{a}{t}\right)^2 + M_3\left(\frac{a}{t}\right)^4\right] f_\phi g f_w \tag{4}$$

where

$$M_1 = 1.13 - 0.09\left(\frac{a}{c}\right) \tag{5}$$

$$M_2 = -0.54 + \frac{0.89}{0.2 + \frac{a}{c}} \tag{6}$$

$$M_3 = 0.5 - \frac{1.0}{0.65 + \frac{a}{c}} + 14\left(1.0 - \frac{a}{c}\right)^{24} \tag{7}$$

$$g = 1 + \left[0.1 + 0.35\left(\frac{a}{t}\right)^2\right](1 - \sin\phi)^2 \tag{8}$$

The function f_ϕ, an angular function from the embedded elliptical-crack solution (ref. 9), is

$$f_\phi = \left[\left(\frac{a}{c}\right)^2 \cos^2\phi + \sin^2\phi\right]^{1/4} \tag{9}$$

The function f_w, a finite-width correction from reference 12, is

$$f_w = \left[\sec\left(\frac{\pi c}{2b}\sqrt{\frac{a}{t}}\right)\right]^{1/2} \tag{10}$$

The function H, developed herein also by curve fitting and engineering judgment, has the form

$$H = H_1 + (H_2 - H_1)\sin^p\phi \tag{11}$$

where

$$p = 0.2 + \frac{a}{c} + 0.6\frac{a}{t} \tag{12}$$

$$H_1 = 1 - 0.34\frac{a}{t} - 0.11\frac{a}{c}\left(\frac{a}{t}\right) \tag{13}$$

$$H_2 = 1 + G_1\left(\frac{a}{t}\right) + G_2\left(\frac{a}{t}\right)^2 \tag{14}$$

In this equation for H_2,

$$G_1 = -1.22 - 0.12\frac{a}{c} \tag{15}$$

$$G_2 = 0.55 - 1.05\left(\frac{a}{c}\right)^{0.75} + 0.47\left(\frac{a}{c}\right)^{1.5} \tag{16}$$

For all combinations of parameters investigated and $a/t \leq 0.8$, equation (2) was within ±5 percent of the finite-element results and the single-edge crack solution. (Herein, "percent error" is defined as the difference between equation (2) and the finite-element results normalized by the maximum value for that particular case. This definition is necessary, especially for the case of bending, for which the stress-intensity factor ranges from positive to negative along the crack front.) For $a/t > 0.8$, the accuracy of equation (2) has not been established. However, its use in that range appears to be supported by estimates based on the concept of an equivalent through crack. Results from equation (2) for tension and bending are shown in figures 10 and 11, respectively, with the stress-intensity factor plotted as a function of ϕ for several combinations of a/c and a/t to illustrate the characteristics of the equation.

Equation (2) is used in appendix A to predict the growth patterns of surface cracks under tension and bending fatigue loads. The predicted growth patterns are in fair to good agreement with previously published experimental measurements made on steel, titanium alloy, and aluminum alloy material. A modified form of equation (2) is also used in appendix B to correlate surface-crack fracture data from the literature for a brittle epoxy material under tension loads. In these data, the ratios of crack depth to plate thickness ranged from 0.15 to 1.0 and the ratios of crack depth to crack length ranged from 0.3 to 0.84. The equation correlated 95 percent of the data analyzed to within ±10 percent of the calculated failure stress.

CONCLUDING REMARKS

A three-dimensional, finite-element stress analysis was used to calculate mode I stress-intensity factor variations along the crack front for a wide range of semielliptical surface cracks in finite elastic plates subjected to remote tension or bending loads.

For remote tension, the maximum stress-intensity factor occurs at the maximum depth point for small ratios of crack depth to crack length and at the intersection of the crack with the front surface for large ratios. For remote bending, the maximum value occurs at the intersection of the crack with the front surface for ratios of crack depth to plate thickness greater than or equal to 0.6, regardless of the ratio of crack depth to crack length. For the lowest ratio of crack depth to plate thickness considered (0.2), the stress-intensity factor variations along the crack front were similar in the tension and bending cases. Also, larger ratios of crack length to plate width give higher stress-intensity factors for both tension and bending loads.

The finite-element results are used to develop a wide-range equation for stress-intensity factor for both tension and bending loads. The equation applies for any parametric angle, ratios of crack depth to crack length ranging from 0 to 1.0, ratios of crack depth to plate thickness ranging from 0 to 1.0, and ratios of crack length to plate width less than 0.5. For all configurations for which ratios of crack depth to plate thickness do not exceed 0.8, the equation is within ±5 percent of the finite-element results and the single-edge crack solution. For ratios greater than 0.8, no solutions are available for direct comparison; however, the equation appears reasonable on the basis of engineering estimates.

The wide-range equation is used in appendix A to predict the growth patterns of surface cracks under tension and bending fatigue loads. The predicted growth patterns were in fair to good agreement with previously published experimental measurements made on steel, titanium alloy, and aluminum alloy material. A modified form of the equation is also used in appendix B to correlate surface-crack fracture data from the literature on a brittle epoxy material. In these data, the ratios of crack depth to plate thickness ranged from 0.15 to 1.0 and the ratios of crack depth to crack length ranged from 0.3 to 0.84. The equation correlated 95 percent of the data analyzed to within ±10 percent of the calculated failure stress.

The stress-intensity factor equations presented herein should be useful for correlating fatigue-crack-growth rates as well as in computing fracture toughness of surface-cracked plates.

Langley Research Center
National Aeronautics and Space Administration
Hampton, VA 23665
November 19, 1979

APPENDIX A

FATIGUE-CRACK-GROWTH PATTERNS OF SURFACE CRACKS

The stress-intensity factor equation (eq. (2)) developed for surface cracks is used herein to predict fatigue-crack-growth patterns under tension and bending fatigue loads. The predicted growth patterns are compared with experimental data obtained from the literature for steels, titanium alloys, and aluminum alloys.

Procedure

The surface-crack configuration considered is shown in figure 1. Although equation (2) gives the stress-intensity factor at any location along the crack front, only the values at the maximum-depth point A and at the front surface B were used to predict the crack-growth patterns. (See inset in fig. 1.) The cracks were always assumed to be semielliptical with semiaxes a and c.

The crack-growth rates were calculated by assuming that the Paris relationship (ref. 13) between crack-growth rate and stress-intensity factor range is obeyed independently at points A and B at the crack front. Thus,

$$\frac{da}{dN} = C_A \Delta K_A^n \tag{A1}$$

$$\frac{dc}{dN} = C_B \Delta K_B^n \tag{A2}$$

where ΔK is the stress-intensity factor range at point A or B, n is an exponent to be specified, and C_A and C_B are the crack-growth coefficients for points A and B, respectively. In this paper, n is assumed to be 4, a value which has been found to be applicable to a wide range of materials. Normally, C_A and C_B are assumed to be equal; however, experimental results (refs. 14 and 15) for surface cracks under tension and bending fatigue loads show that small semicircular cracks tend to grow semicircular for low a/t ratios. Because the stress-intensity factor solution for the small semicircular crack (table I) shows that the stress intensity at point B is about 10 percent higher than the value at point A, the coefficient C_B was assumed to be

$$C_B = 0.9^n C_A \tag{A3}$$

so that a small semicircular crack would be predicted to initially retain its shape. Accordingly, equation (A3) was used for all crack configurations con-

sidered. One reason C_A is not equal to C_B may be the changing relationship between the stress-intensity factor and the crack-growth rate as the stress state changes from plane stress on the front surface to plane strain at the maximum-depth point.

The number of stress cycles required for propagation of a surface crack from an initial half-length c_o to a desired half-length c_f was obtained by a numerical integration of equation (A2). This was accomplished by dividing the crack extension $(c_f - c_o)$ into a large number of equal increments Δc and assuming that each increment was created at a constant crack-growth rate. The constant growth rate for each increment was determined from equation (A2) by using the crack configuration which existed at the start of that growth increment. For each increment of crack advance Δc at the surface, a new increment of crack depth Δa was computed from

$$\Delta a = \frac{C_A}{C_B}\left(\frac{\Delta K_A}{\Delta K_B}\right)^n \Delta c = \left(\frac{\Delta K_A}{0.9\Delta K_B}\right)^n \Delta c \qquad \text{(A4)}$$

This defined the crack configuration for the next growth increment, and the process was repeated until the crack depth reached the plate thickness.

Tension

Figure 12 shows the experimental and predicted fatigue-crack-growth patterns for surface cracks subjected to tension. The figure shows the a/c ratio plotted against the a/t ratio for Ti-6Al-4V titanium alloy (ref. 16), 9-percent nickel steel (ref. 17), and 2219-T87 aluminum alloy.

The experimental procedure for the aluminum and titanium alloys was as follows. An electric-discharge machined (EDM) notch was used as a crack starter. The vertical bar in figure 12 denotes the range of EDM notch shapes (a/c) for the nine aluminum-alloy specimens. Each specimen was subjected to constant-amplitude cyclic loading for various numbers of cycles and then statically pulled to failure. The data points indicate the final fatigue-crack shapes and sizes measured from the broken specimens. Hence, a separate specimen was necessary to obtain each data point.

The experimental data for the nickel steel were obtained from one specimen which was subjected to two-level variable-amplitude loading and then pulled to failure. The amplitude change caused "marker bands" to be formed on the crack plane. The marker bands in turn were used to define the crack shape and size.

The dashed curves in figure 12 are the predicted fatigue-crack-growth patterns from equation (2) and equations (A1) to (A4). (Note that n is assumed to be equal to 4 and that the growth patterns are independent of the magnitude of C_A and C_B. See eq. (A4).) The predicted growth patterns are in good agreement with the measurements made on the three materials. The solid symbols denote initial crack size and shape. For all initial crack shapes con-

sidered, the predicted a/c ratio was about 0.8 when the crack depth became equal to the plate thickness.

Bending

Figures 13 and 14 show the experimental and predicted fatigue-crack-growth patterns for surface cracks in plates subjected to cantilever bending. Although the stress-intensity factor equation (eq. (2)) used herein was developed for pure bending, the differences between crack-growth patterns for cantilever and pure bending are not expected to be large. The a/c ratio is plotted as a function of the a/t ratio for aluminum-alloy specimens in figure 13 and steel specimens in figure 14. All data points for the 2014-T651 aluminum alloy (ref. 14) were obtained from separate specimens, whereas most of the data on the T-1 steel (ref. 18) and carbon steel (SS41) (ref. 17) were obtained from single specimens. The aluminum-alloy specimens were cycled under constant-amplitude loading and then statically pulled to failure, whereas the steel specimens were cycled under two-level variable-amplitude loading. The two-level loading produced marker bands on the crack plane from which the experimental data were obtained. Again, the solid symbols denote the initial crack dimensions.

In figure 13, the predicted fatigue-crack-growth patterns (dashed curves) are in good agreement with the experimental data for the aluminum alloy. The predicted results show that the cracks tended to approach a common propagation pattern, as pointed out by Corn (ref. 14).

In figure 14, the solid curves are drawn through the T-1 steel data and the symbols show the carbon-steel data. Here, the predicted growth patterns (dashed curves) are in disagreement with the experimental data for the T-1 steel. Although the trends are similar, the predicted curves are as much as 40-percent higher than the experimental curves for T-1 steel, whereas the predicted curve for the carbon steel is about 15-percent lower than the experimental data (symbols).

This disagreement between predicted and measured growth patterns for the steels prompted a search for additional data. Figure 15 shows fatigue-crack-growth patterns measured for H-11 steel (ref. 15), 4340 steel (ref. 15), D6-AC steel (ref. 19), Ti-6Al-4V titanium alloy (ref. 19), 2014-T651 aluminum alloy (ref. 14), and the T-1 steel (ref. 18). Again, solid curves were drawn through the experimental data. These results show a systematic thickness effect; that is, the crack shape (a/c) is generally less for thicker material at a given a/t ratio. The upper solid curve (H-11 and 4340 steel) is for the thinnest material considered (t = 1.8 mm), whereas the lowest solid curve (T-1 steel) is for the thickest material (t = 25.4 mm). The titanium alloy and the D6-AC steel were 6.4 mm thick, the carbon steel was 10 mm thick, and the 2014-T651 aluminum alloy was 9.5 mm thick.

This thickness-related trend may be due to the presence of residual stresses in the surface layer (ref. 20). Tensile residual stresses in the surface layer will cause higher stress-intensity factors on the surface than factors calculated from equation (2); hence, crack growth will be more rapid at the surface. Thus, the a/c ratios will be lower than those predicted for

a given value of a/t. In contrast, compressive residual stresses in the surface layer would cause cracks to grow more slowly on the surface than predicted by equation (2). This would cause higher a/c ratios than those predicted for a given value of a/t.

The dashed curve in figure 15 shows the results predicted by using equations (2), (A1), and (A2). The predicted-results curve was roughly the average of all of the experimental data.

APPENDIX B

FRACTURE OF SURFACE-CRACKED BRITTLE MATERIALS

The stress-intensity factor solutions for surface cracks and for single-edge cracks (ref. 10) in plates subjected to tension are used herein to develop an equation for fracture of surface-cracked brittle materials. The equation is used to correlate fracture data for a wide range of crack shapes and sizes in surface-cracked tension specimens made of a brittle epoxy material.

Stress-Intensity Factor Equation for Fracture

The application of linear-elastic fracture mechanics to surface-cracked specimens is complicated by the fact that the stress-intensity factor solution is a function of the parametric angle ϕ. For surface cracks with $a/c < 0.6$, the maximum stress-intensity factor occurs at the maximum-depth point, $\phi = \pi/2$; for surface cracks with $a/c \geq 0.6$, the maximum stress-intensity factor occurs near the front surface $\phi = 0$. In fracture analyses, most investigators have used the stress-intensity factor at the maximum-depth point (ref. 11). However, for a/c ratios greater than about 0.6, some investigators have used the value at the front surface because the stress-intensity factor is maximum there. When the stress-intensity factor is maximum at the front surface, it may not control fracture. The surface material is more nearly in a state of plane stress; hence, its resistance to fracture is higher there than in the interior, where nearly plane-strain conditions prevail. Thus, for a/c ratios greater than about 0.6, fracture may initiate near, though not necessarily at, the front surface.

In this paper, the maximum stress-intensity factor for $a/c < 0.6$ and an "average" value for $0.6 \leq a/c \leq 1.0$ are used to develop an equation for predicting fracture. The average stess-intensity factor is the average between the values at $\phi = 0$ and at $\pi/2$. For a/c ratios greater than 1.0, an engineering estimate similar to that in reference 21 is used.

For convenience of application, an equation was developed to fit these numerical results. The equation is essentially an extension of an equation presented in reference 21. Details of the extension, which involved engineering judgment combined with a considerable amount of trial and error, are largely omitted. The elastic stress-intensity factor at failure was taken as

$$K_{Ie} = S_t\sqrt{\frac{\pi a}{Q}}\,M_e \qquad \text{(B1)}$$

for $0.03 \leq a/c < \infty$, $0 \leq a/t < 1.0$, and $c/b < 0.5$. The remote stress is S_t; M_e, the elastic magnification factor, is

APPENDIX B

$$M_e = \left[M_1 + \left(\sqrt{Q \frac{c}{a}} - M_1 \right) \left(\frac{a}{t} \right)^p + \sqrt{Q \frac{c}{a}} \, (M_2 - 1) \left(\frac{a}{t} \right)^{2p} \right] f_w \tag{B2}$$

where $p = \sqrt{\pi}$. The shape factor Q is approximated by

$$\left.\begin{aligned} Q &= 1 + 1.464\left(\frac{a}{c}\right)^{1.65} && \left(\frac{a}{c} \leq 1\right) \\ Q &= 1 + 1.464\left(\frac{c}{a}\right)^{1.65} && \left(\frac{a}{c} > 1\right) \end{aligned}\right\} \tag{B3}$$

The factors M_1 and M_2 are expressed as

$$\left.\begin{aligned} M_1 &= 1.13 - 0.1\left(\frac{a}{c}\right) && \left(0.03 \leq \frac{a}{c} \leq 1\right) \\ M_1 &= \sqrt{\frac{c}{a}}\left[1 + 0.03\left(\frac{c}{a}\right)\right] && \left(\frac{a}{c} > 1\right) \end{aligned}\right\} \tag{B4}$$

and

$$\left.\begin{aligned} M_2 &= \sqrt{\frac{\pi}{4}} && \left(\frac{a}{c} \leq 1\right) \\ M_2 &= 1 + \frac{c}{a}\left(\sqrt{\frac{\pi}{4}} - 1\right) && \left(\frac{a}{c} > 1\right) \end{aligned}\right\} \tag{B5}$$

The finite-width correction f_w, obtained from reference 12, is

$$f_w = \left[\sec\left(\frac{\pi c}{2b} \sqrt{\frac{a}{t}} \right) \right]^{1/2} \tag{B6}$$

APPENDIX B

For $a/c < 0.03$, the stress-intensity factor for the single-edge crack plate subjected to tension (ref. 10) was assumed to apply, and M_e was written as

$$M_e = \sqrt{Q}\left[1.12 - 0.23\left(\frac{a}{t}\right) + 10.55\left(\frac{a}{t}\right)^2 - 21.71\left(\frac{a}{t}\right)^3 + 30.38\left(\frac{a}{t}\right)^4\right] \tag{B7}$$

Analysis of Fracture Data

Equation (B1) has been used to analyze data obtained by Smith (ref. 22) in a large number of fracture tests on surface-cracked tension specimens made of a brittle epoxy material. (Plane-strain plastic-zone size, based on the largest computed fracture toughness, was two orders of magnitude below minimum specimen thickness and, hence, consistent with brittle fracture behavior.) Thicknesses ranged from 2.5 to 9.5 mm, with $0.15 \leqq a/t \leqq 1.0$ and $0.3 \leqq a/c \leqq 0.84$. All specimens were 25 mm wide.

In this analysis, the specimens were arranged into five groups according to their date of manufacture. Specimen thicknesses were constant within each group. Fracture of all specimens was assumed to occur at the same value of stress-intensity factor (denoted herein by K_{cr}). The elastic fracture toughness K_{cr} for each group of specimens was obtained by averaging the calculated stress-intensity factors at failure K_{Ie} as

$$K_{cr} = \frac{1}{m}\sum_{i=1}^{m}(K_{Ie})_i \tag{B8}$$

where m is the number of specimens in a group. The K_{cr} values for the five groups of specimens were calculated as 677, 682, 713, 723, and 731 $kN/m^{3/2}$.

After K_{cr} had been determined, equation (B1) was used to calculate failure stresses. The gross failure stresses S_{cal} were calculated from

$$S_{cal} = \frac{K_{cr}}{\sqrt{\pi \frac{a}{Q}}\, M_e} \tag{B9}$$

Figure 16 shows the ratio of experimental failure stress S_{exp} to calculated failure stress S_{cal} plotted as a function of the a/t ratio. The solid line at unity denotes perfect agreement and the dashed lines denote ±10-percent scat-

ter. The proposed equation correlated 95 percent of the data analyzed within ±10 percent for a wide range of a/t and a/c ratios.

REFERENCES

1. Smith, F. W.; and Alavi, M. J.: Stress Intensity Factors for a Penny Shaped Crack in a Half Space. Eng. Fract. Mech., vol. 3, no. 3, Oct. 1971, pp. 241-254.

2. Smith, F. W.; and Sorensen, D. R.: Mixed Mode Stress Intensity Factors for Semielliptical Surface Cracks. NASA CR-134684, 1974.

3. Kobayashi, A. S.; Polvanich, N.; Emery, A. F.; and Love, W. J.: Surface Flaws in a Plate in Bending. Proceedings 12th Annual Meeting of the Society of Engineering Science, Oct. 1975, pp. 343-352.

4. Kathiresan, K.: Three-Dimensional Linear Elastic Fracture Mechanics Analysis by a Displacement Hybrid Finite Element Model. Ph. D. Thesis, Georgia Inst. of Tech., 1976.

5. Raju, I. S.; and Newman, J. C., Jr.: Improved Stress-Intensity Factors for Semi-Elliptical Surface Cracks in Finite-Thickness Plates. NASA TM X-72825, 1977.

6. Raju, I. S.; and Newman, J. C., Jr.: Stress-Intensity Factors for a Wide Range of Semi-Elliptical Surface Cracks in Finite-Thickness Plates. Eng. Fract. Mech., vol. 11, no. 4, 1979, pp. 817-829.

7. Raju, I. S.; and Newman, J. C., Jr.: Three-Dimensional Finite-Element Analysis of Finite-Thickness Fracture Specimens. NASA TN D-8414, 1977.

8. Tracey, D. M.: Finite Elements for Three-Dimensional Elastic Crack Analysis. Nucl. Eng. & Des., vol. 26, no. 2, 1974, pp. 282-290.

9. Green, A. E.; and Sneddon, I. N.: The Distribution of Stress in the Neighbourhood of a Flat Elliptical Crack in an Elastic Solid. Proc. Cambridge Philos. Soc., vol. 46, pt. 1, Jan. 1950, pp. 159-163.

10. Gross, Bernard; and Srawley, John E.: Stress-Intensity Factors for Single-Edge-Notch Specimens in Bending or Combined Bending and Tension by Boundary Collocation of a Stress Function. NASA TN D-2603, 1965.

11. Merkle, J. G.: A Review of Some of the Existing Stress Intensity Factor Solutions for Part-Through Surface Cracks. ORNL-TM-3983, U. S. At. Energy Comm., Jan. 1973.

12. Newman, J. C., Jr.: Predicting Failure of Specimens With Either Surface Cracks or Corner Cracks at Holes. NASA TN D-8244, 1976.

13. Paris, Paul C.: The Fracture Mechanics Approach to Fatigue. Fatigue - An Interdisciplinary Approach, John J. Burke, Norman L. Reed, and Volker Weiss, eds., Syracuse Univ. Press, 1964, pp. 107-132.

14. Corn, D. L.: A Study of Cracking Techniques for Obtaining Partial Thickness Cracks of Pre-Selected Depths and Shapes. Eng. Fract. Mech., vol. 3, no. 1, July 1971, pp. 45-52.

15. Yen, C. S.; and Pendleberry, S. L.: Technique for Making Shallow Cracks in Sheet Metals. Mater. Res. Stand., vol. 2, no. 11, Nov. 1962, pp. 913-916.

16. Hoeppner, David W.; Pettit, Donald E.; Feddersen, Charles E.; and Hyler, Walter S.: Determination of Flaw Growth Characteristics of Ti-6Al-4V Sheet in the Solution-Treated and Aged Condition. NASA CR-65811, 1968.

17. Nishioka, Kunio; Hirakawa, Kenji; and Kitaura, Ikushi: Fatigue Crack Propagation Behaviors of Various Steels. The Sumitomo Search No. 17, May 1977, pp. 39-55. (Available as ICAF-993.)

18. Pierce, W. S.; and Shannon, J. L., Jr.: Surface-Crack Shape Change in Bending Fatigue Using an Inexpensive Resonant Fatiguing Apparatus. J. Test. & Eval., vol. 6, no. 3, May 1978, pp. 183-188.

19. Randall, P. N.: Severity of Natural Flaws as Fracture Origins and a Study of the Surface-Cracked Specimen. AFML-TR-66-204, U.S. Air Force, Aug. 1966. (Available from DDC as AD 487 986.)

20. Elber, Wolf: Effects of Shot-Peening Residual Stresses on the Fracture and Crack-Growth Properties of D6AC Steel. Fracture Toughness and Slow-Stable Cracking. Spec. Tech. Publ. 559, American Soc. Testing & Mater., 1974, pp. 45-58.

21. Newman, J. C., Jr.: Fracture Analysis of Surface- and Through-Cracked Sheets and Plates. Eng. Fract. Mech., vol. 5, no. 3, Sept. 1973, pp. 667-689.

22. Smith, F. W.: The Elastic Analysis of the Part-Circular Surface Flaw Problem by the Alternating Method. The Surface Crack: Physical Problems and Computational Solutions, J. L. Swedlow, ed., c.1972, pp. 125-152.

TABLE I.- NORMALIZED STRESS-INTENSITY FACTORS FOR A SURFACE CRACK IN A LARGE PLATE UNDER TENSION OR BENDING LOADS

$[c/b = 0.2;\ c/h = 0.2;\ \nu = 0.3]$

a/c	$2\phi/\pi$	Normalized stress-intensity factors for a/t of -							
		0.2	0.4	0.6	0.8	0.2	0.4	0.6	0.8
		Tension				Bending			
0.2	0	0.617	0.724	0.899	1.190	0.572	0.629	0.701	0.787
	.125	.650	.775	.953	1.217	.583	.625	.669	.722
	.250	.754	.883	1.080	1.345	.648	.655	.669	.686
	.375	.882	1.009	1.237	1.504	.728	.693	.678	.656
	.500	.990	1.122	1.384	1.657	.787	.716	.672	.601
	.625	1.072	1.222	1.501	1.759	.825	.728	.649	.521
	.750	1.128	1.297	1.581	1.824	.847	.731	.619	.427
	.875	1.161	1.344	1.627	1.846	.859	.730	.595	.351
	1.000	1.173	1.359	1.642	1.851	.862	.729	.586	.321
0.4	0	0.767	0.896	1.080	1.318	0.705	0.755	0.798	0.838
	.125	.781	.902	1.075	1.285	.698	.719	.732	.742
	.250	.842	.946	1.113	1.297	.722	.695	.667	.634
	.375	.923	1.010	1.179	1.327	.759	.685	.617	.532
	.500	.998	1.075	1.247	1.374	.789	.672	.565	.426
	.625	1.058	1.136	1.302	1.408	.809	.658	.511	.323
	.750	1.103	1.184	1.341	1.437	.822	.644	.462	.224
	.875	1.129	1.214	1.363	1.446	.828	.633	.428	.150
	1.000	1.138	1.225	1.370	1.447	.830	.629	.416	.123
0.6	0	0.916	1.015	1.172	1.353	0.838	0.851	0.862	0.868
	.125	.919	1.004	1.149	1.304	.817	.799	.779	.753
	.250	.942	1.009	1.142	1.265	.803	.740	.676	.604
	.375	.982	1.033	1.160	1.240	.803	.694	.587	.464
	.500	1.024	1.062	1.182	1.243	.803	.653	.504	.331
	.625	1.059	1.093	1.202	1.245	.802	.616	.430	.213
	.750	1.087	1.121	1.218	1.260	.801	.588	.370	.112
	.875	1.104	1.139	1.227	1.264	.800	.570	.331	.041
	1.000	1.110	1.145	1.230	1.264	.800	.564	.317	.015
1.0	0	1.174	1.229	1.355	1.464	1.076	1.029	1.003	0.964
	.125	1.145	1.206	1.321	1.410	1.021	.956	.894	.821
	.250	1.105	1.157	1.256	1.314	.942	.839	.729	.607
	.375	1.082	1.126	1.214	1.234	.880	.740	.584	.414
	.500	1.067	1.104	1.181	1.193	.831	.655	.458	.241
	.625	1.058	1.088	1.153	1.150	.792	.583	.353	.099
	.750	1.053	1.075	1.129	1.134	.765	.528	.273	-.010
	.875	1.050	1.066	1.113	1.118	.748	.494	.224	-.080
	1.000	1.049	1.062	1.107	1.112	.742	.482	.207	-.104
2.0	0	0.821	0.848	0.866	0.876	0.759	0.720	0.683	0.648
	.125	.794	.818	.833	.839	.709	.648	.587	.526
	.250	.740	.759	.771	.775	.626	.531	.439	.349
	.375	.692	.708	.716	.717	.552	.429	.310	.193
	.500	.646	.659	.664	.661	.486	.343	.202	.063
	.625	.599	.609	.610	.607	.429	.273	.119	-.034
	.750	.552	.560	.560	.554	.379	.221	.062	-.098
	.875	.512	.519	.519	.513	.343	.189	.030	-.132
	1.000	.495	.501	.501	.496	.329	.176	.019	-.141

TABLE II.- NORMALIZED STRESS-INTENSITY FACTORS FOR A SURFACE CRACK IN A FINITE-WIDTH PLATE UNDER TENSION OR BENDING LOADS

[c/h = 0.2; ν = 0.3]

a/c	$2\phi/\pi$	Normalized stress-intensity factors for c/b of -					
		0.4			0.6		0.8
		a/t					
		0.4	0.6	0.8	0.6	0.8	0.8
Tension							
0.2	0	0.743	0.941	1.268	1.037	1.465	1.854
	.125	.794	.993	1.289	1.086	1.474	1.833
	.250	.903	1.120	1.414	1.214	1.595	1.943
	.375	1.030	1.278	1.572	1.374	1.752	2.092
	.500	1.144	1.425	1.720	1.522	1.893	2.216
	.625	1.243	1.540	1.816	1.636	1.976	2.271
	.750	1.319	1.619	1.872	1.712	2.016	2.278
	.875	1.366	1.664	1.888	1.754	2.017	2.253
	1.000	1.381	1.679	1.891	1.768	2.014	2.240
1.0	0	1.293	1.445	1.579	1.660	1.853	2.552
	.125	1.266	1.403	1.512	1.595	1.752	2.334
	.250	1.210	1.326	1.395	1.487	1.588	2.031
	.375	1.174	1.272	1.296	1.408	1.449	1.801
	.500	1.147	1.231	1.239	1.346	1.360	1.632
	.625	1.127	1.195	1.184	1.294	1.277	1.483
	.750	1.110	1.165	1.158	1.252	1.232	1.392
	.875	1.099	1.145	1.137	1.224	1.198	1.330
	1.000	1.095	1.138	1.128	1.215	1.185	1.308
Bending							
0.2	0	0.650	0.733	0.834	0.799	0.941	1.153
	.125	.646	.700	.765	.763	.864	1.058
	.250	.676	.700	.727	.762	.824	1.008
	.375	.715	.710	.695	.773	.791	.968
	.500	.739	.703	.638	.766	.728	.894
	.625	.751	.679	.554	.741	.637	.786
	.750	.753	.648	.455	.707	.528	.660
	.875	.752	.623	.374	.680	.440	.557
	1.000	.751	.613	.343	.670	.406	.518
1.0	0	1.074	1.070	1.058	1.208	1.204	1.574
	.125	.999	.954	.902	1.079	1.030	1.336
	.250	.878	.780	.670	.883	.772	1.006
	.375	.775	.627	.460	.714	.539	.721
	.500	.686	.493	.273	.566	.333	.471
	.625	.611	.382	.119	.443	.164	.267
	.750	.554	.297	.001	.351	.035	.113
	.875	.518	.245	-.075	.294	-.048	.015
	1.000	.506	.228	-.101	.275	-.076	-.019

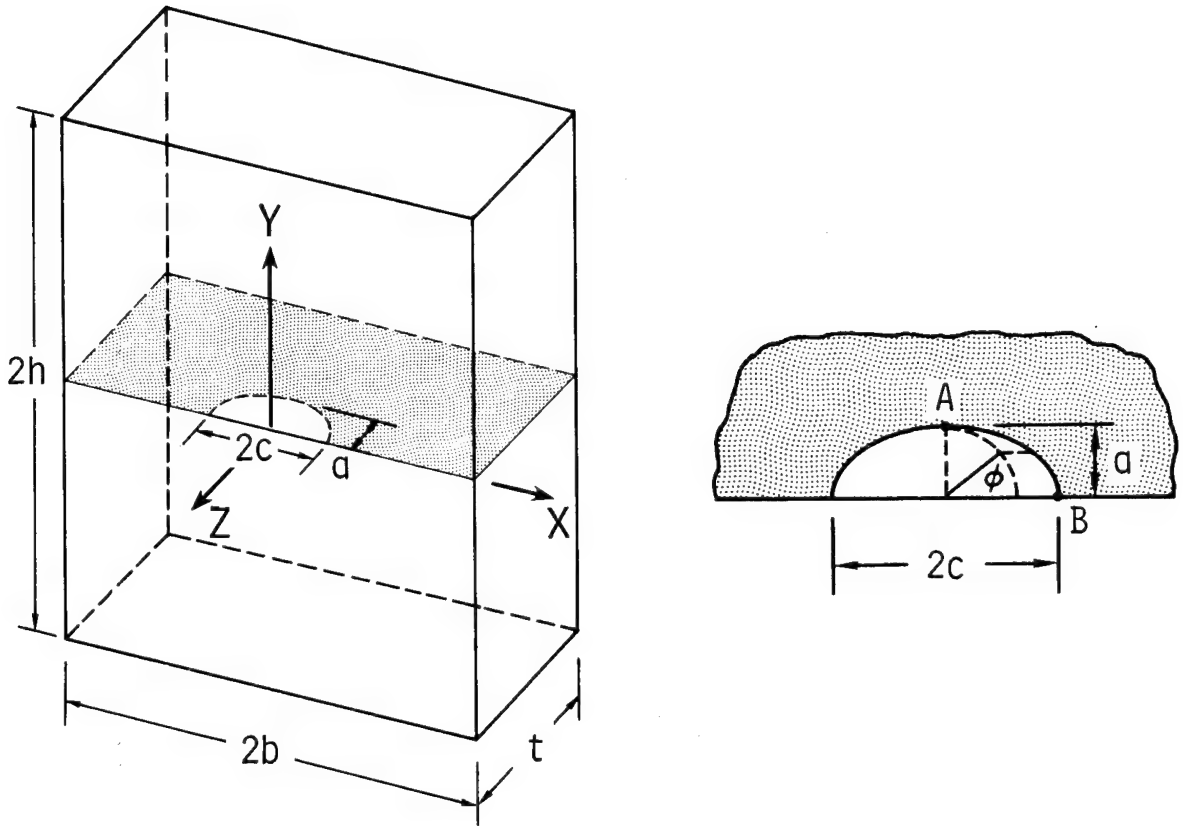

Figure 1.- Surface crack in a finite plate.

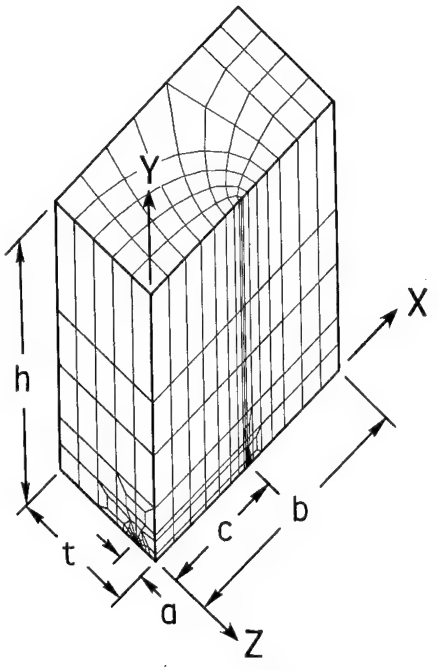

(a) Specimen model.

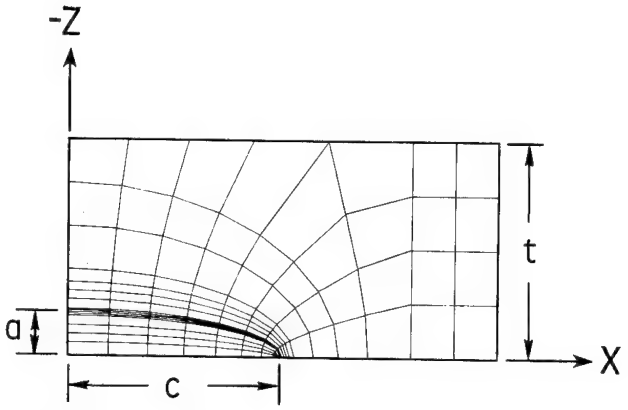

(b) Element pattern on y = 0 plane.

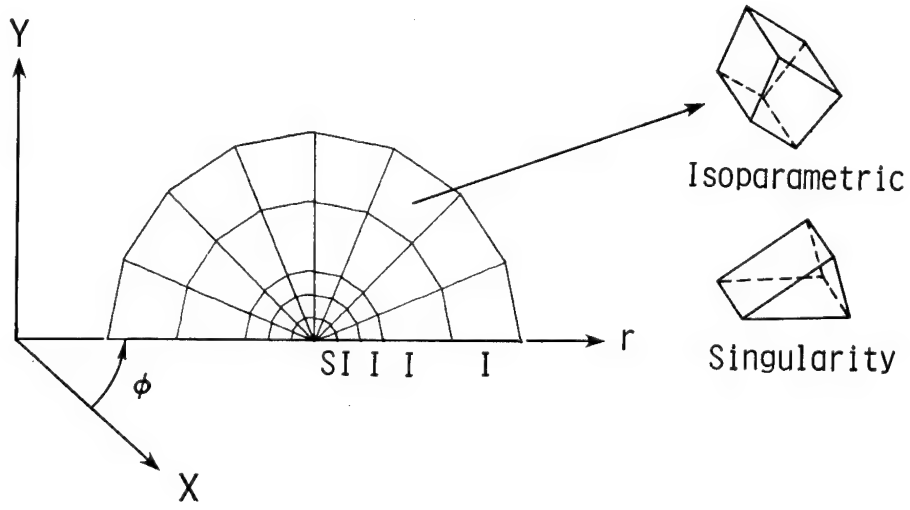

(c) Element pattern around crack front.

Figure 2.- Finite-element model of a plate containing a semielliptical surface crack. (r is the radial coordinate.)

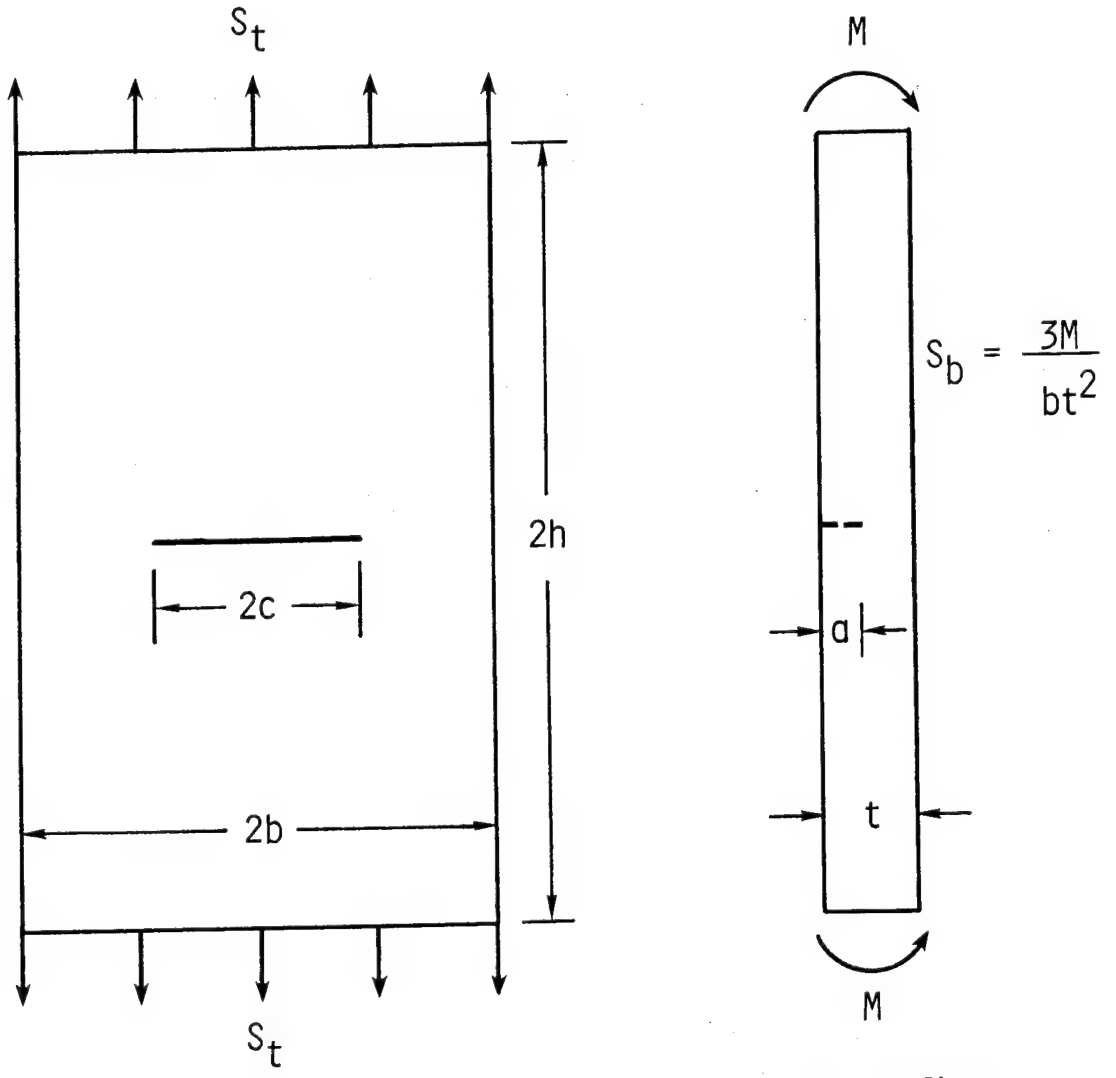

(a) Tension.

(b) Bending.

Figure 3.- Surface-cracked plate subjected to tension or bending loads.

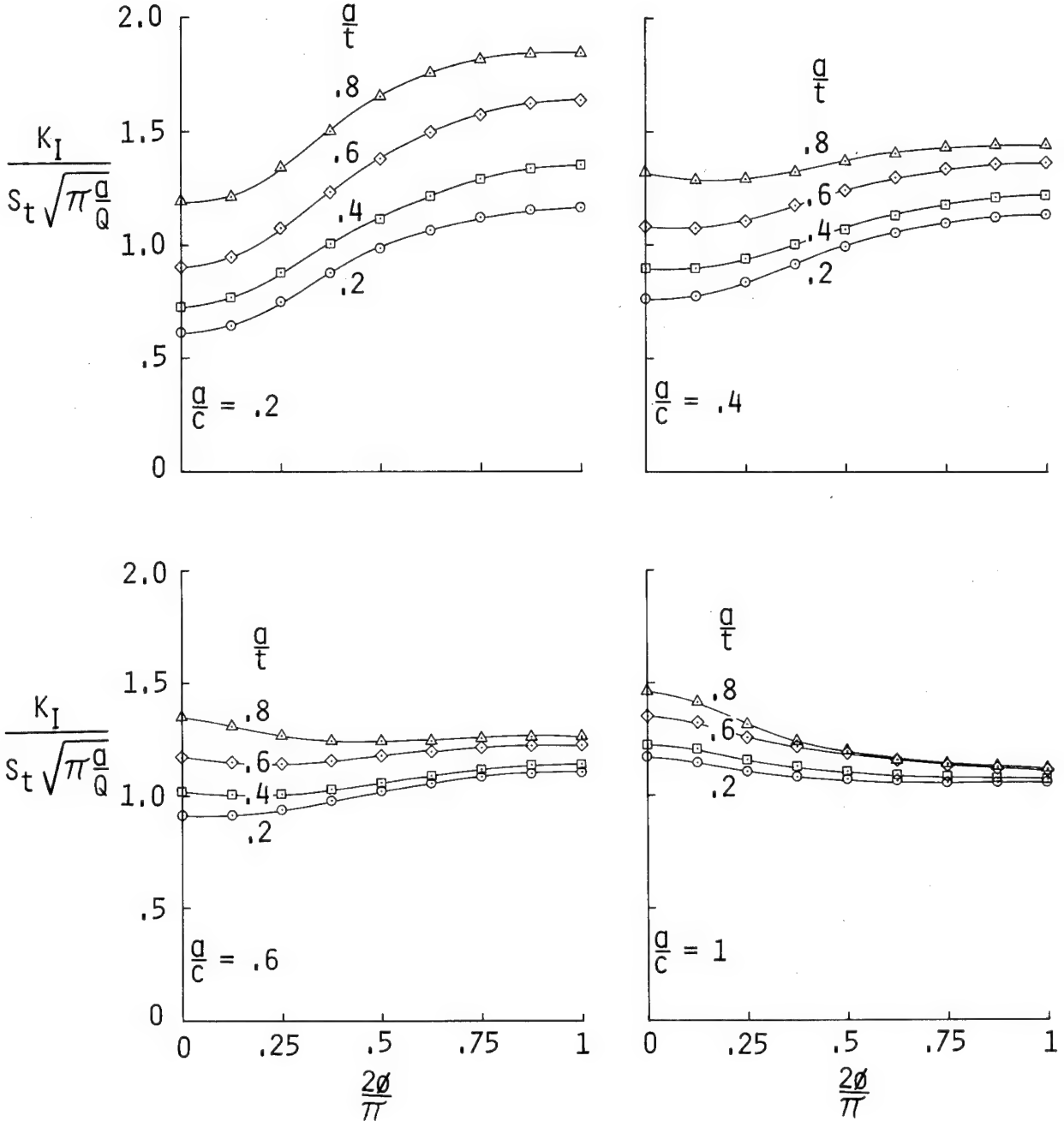

Figure 4.- Normalized stress-intensity factors along the front of a semielliptical surface crack in a plate under tension. (c/b ≦ 0.2.)

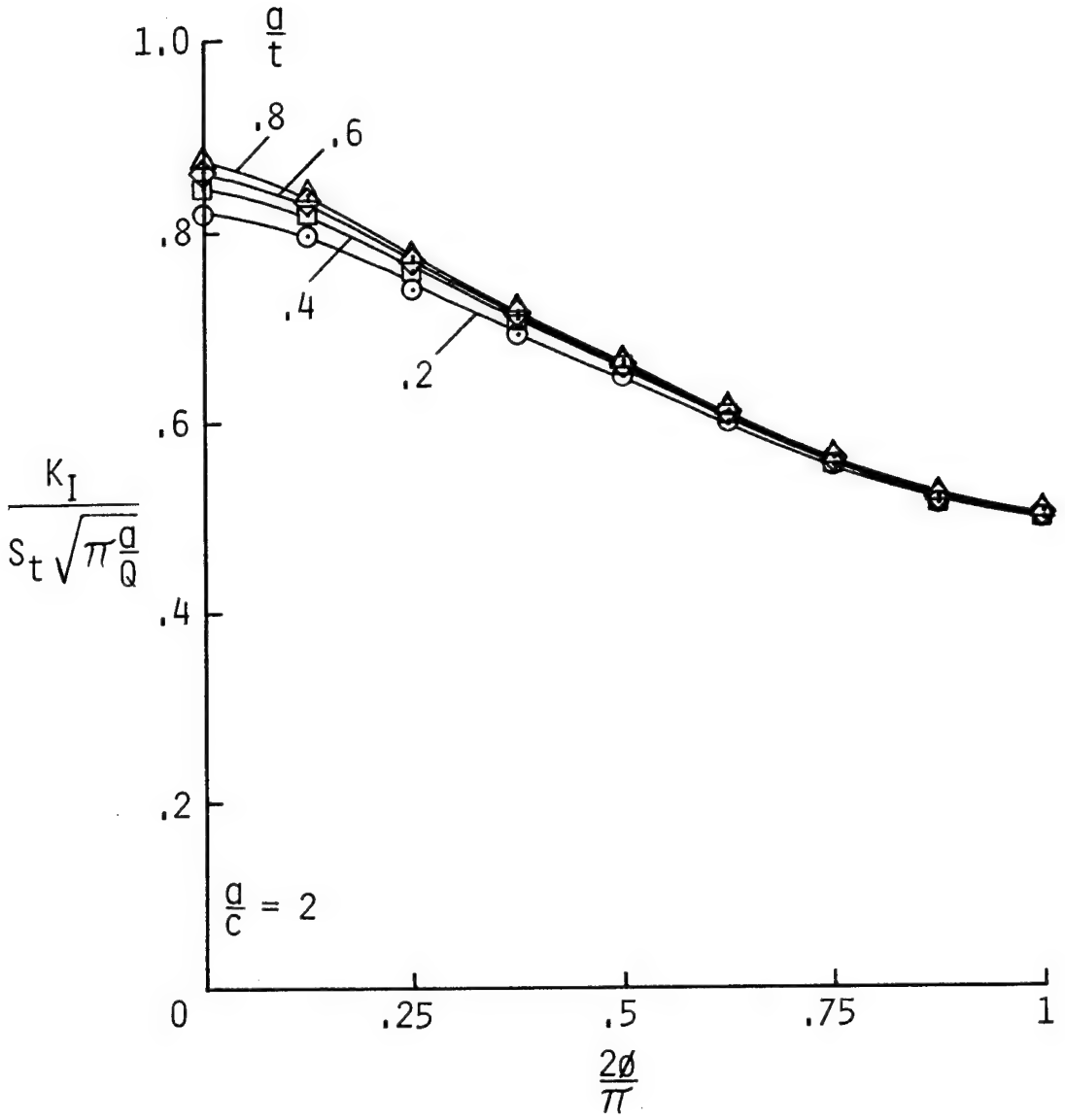

Figure 4.- Concluded.

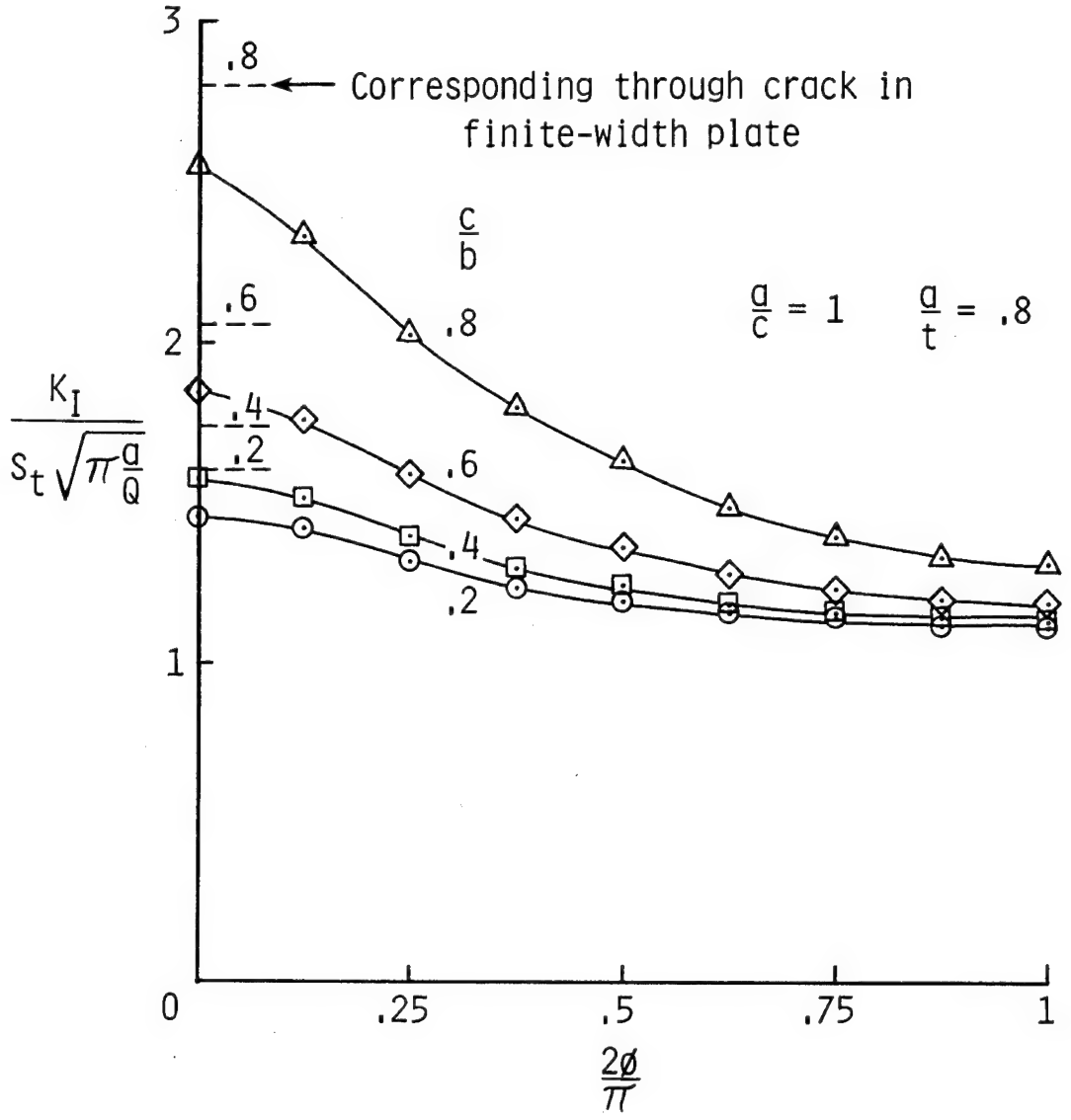

(a) Semicircular crack.

Figure 5.- Normalized stress-intensity factors along the front of a deep surface crack in a plate under tension.

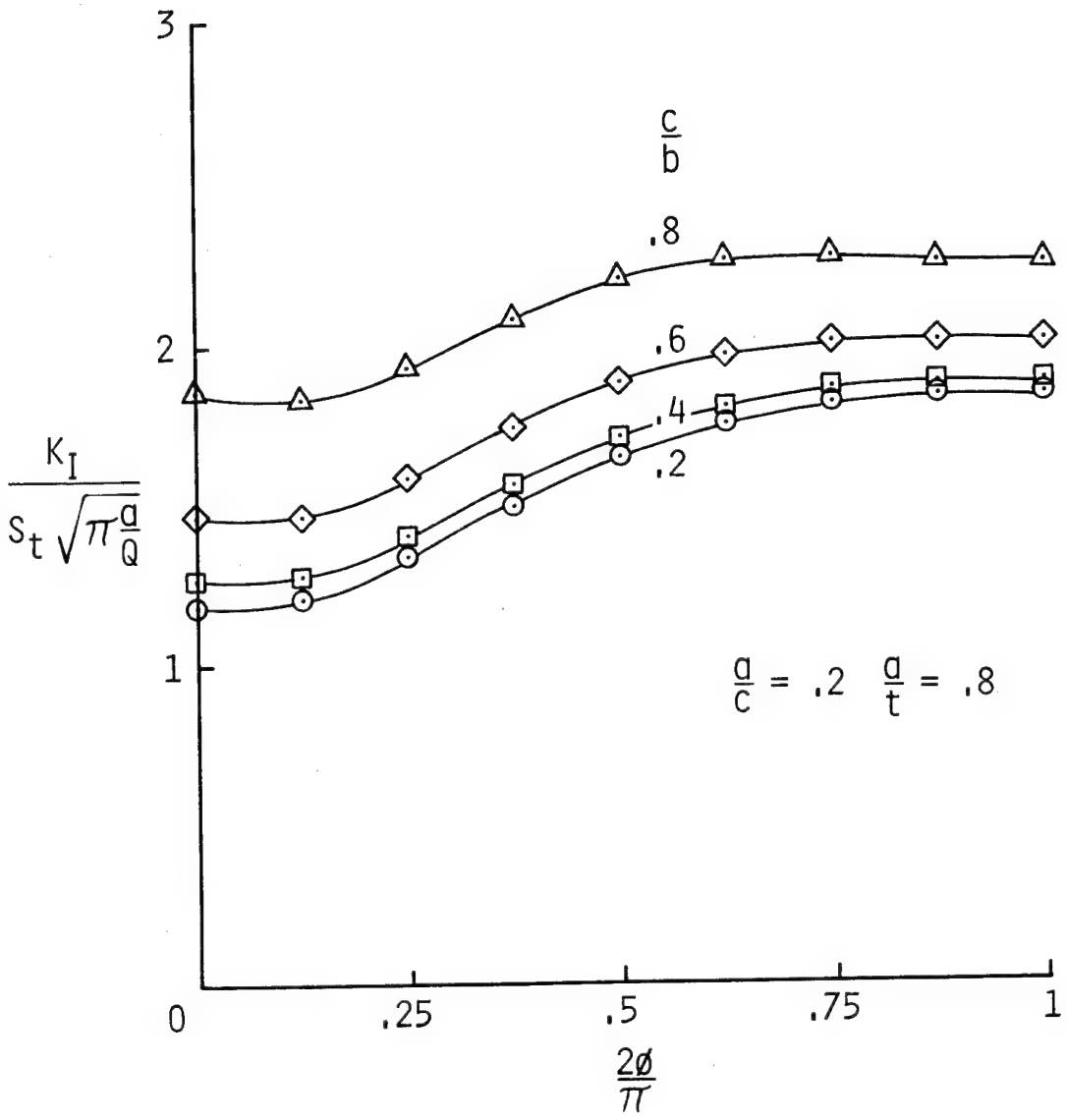

(b) Semielliptical crack.

Figure 5.- Concluded.

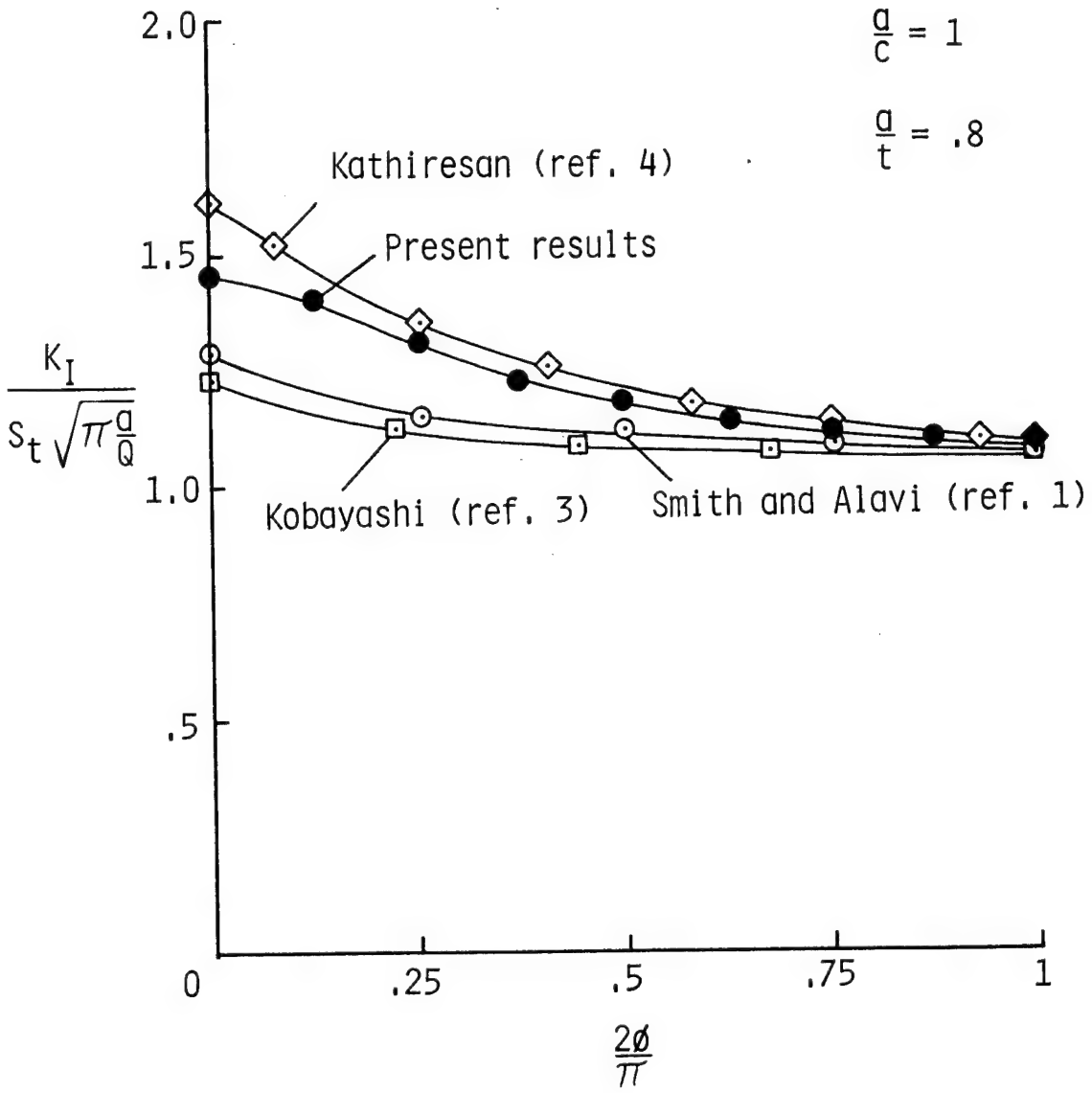

(a) Semicircular crack.

Figure 6.- Comparison of calculated stress-intensity factors with results from the literature for a deep surface crack in a plate under tension.

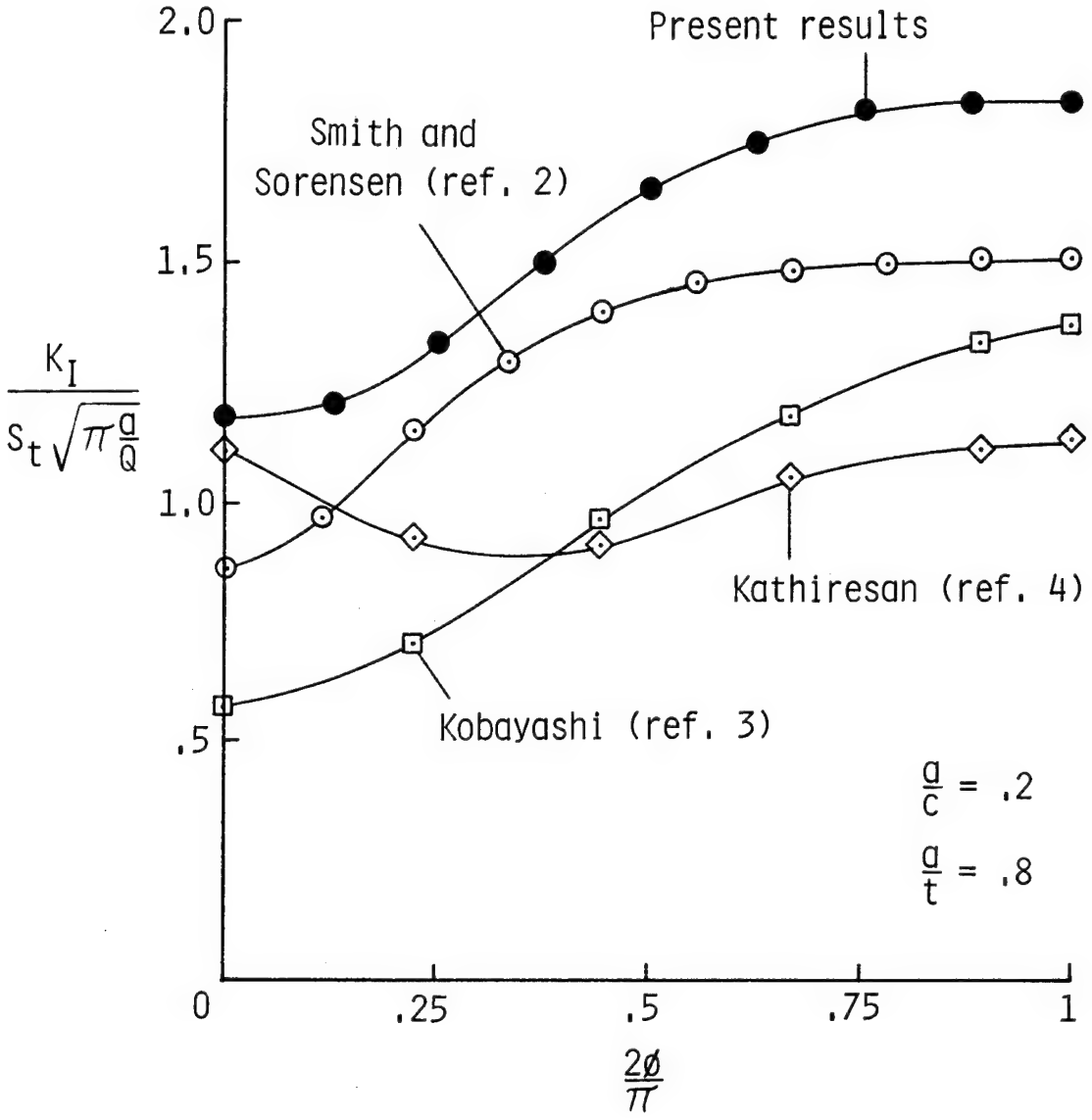

(b) Semielliptical crack.

Figure 6.- Concluded.

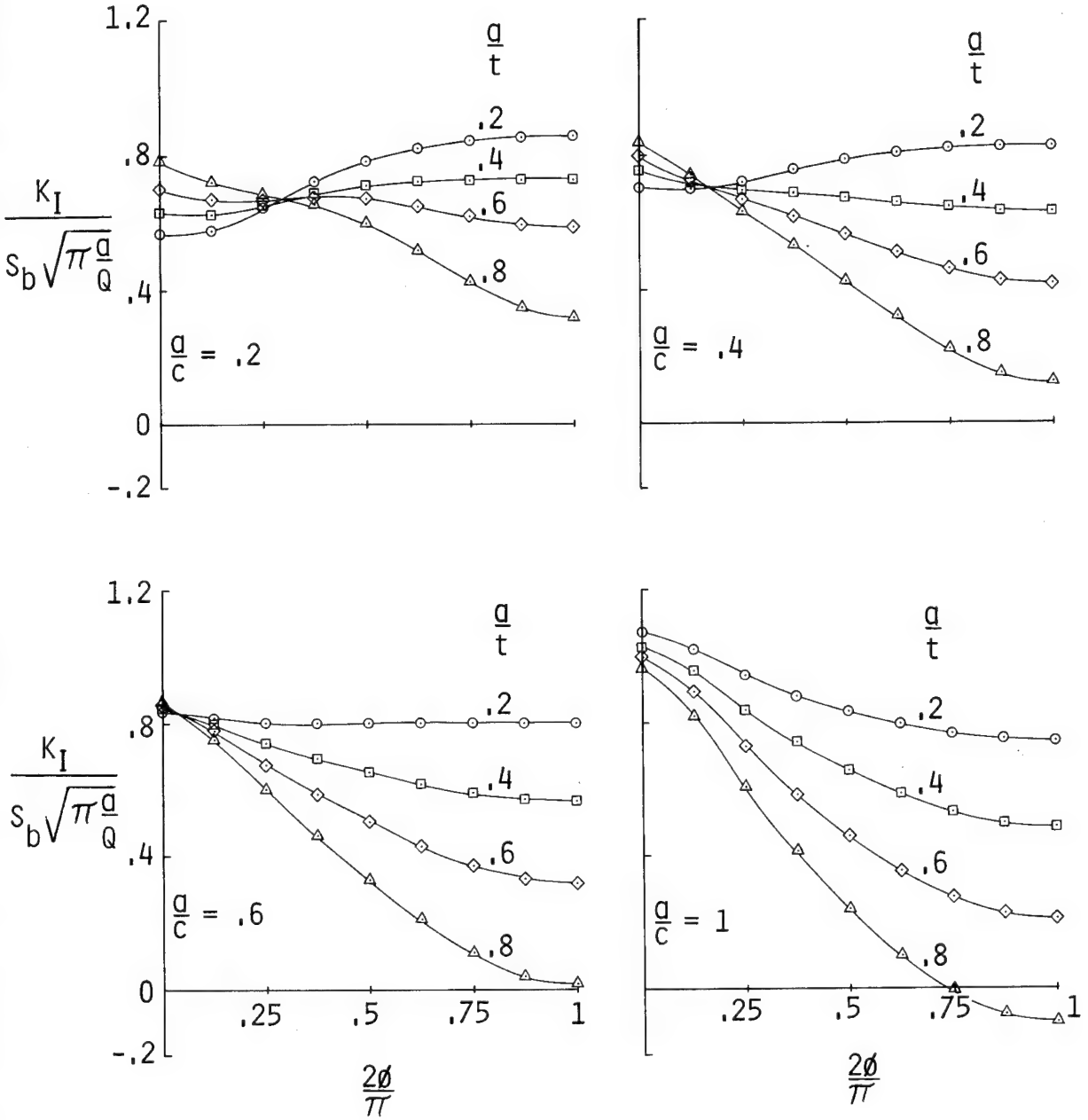

Figure 7.- Normalized stress-intensity factors along the front of a semielliptical surface crack in a plate under bending. (c/b ≦ 0.2.)

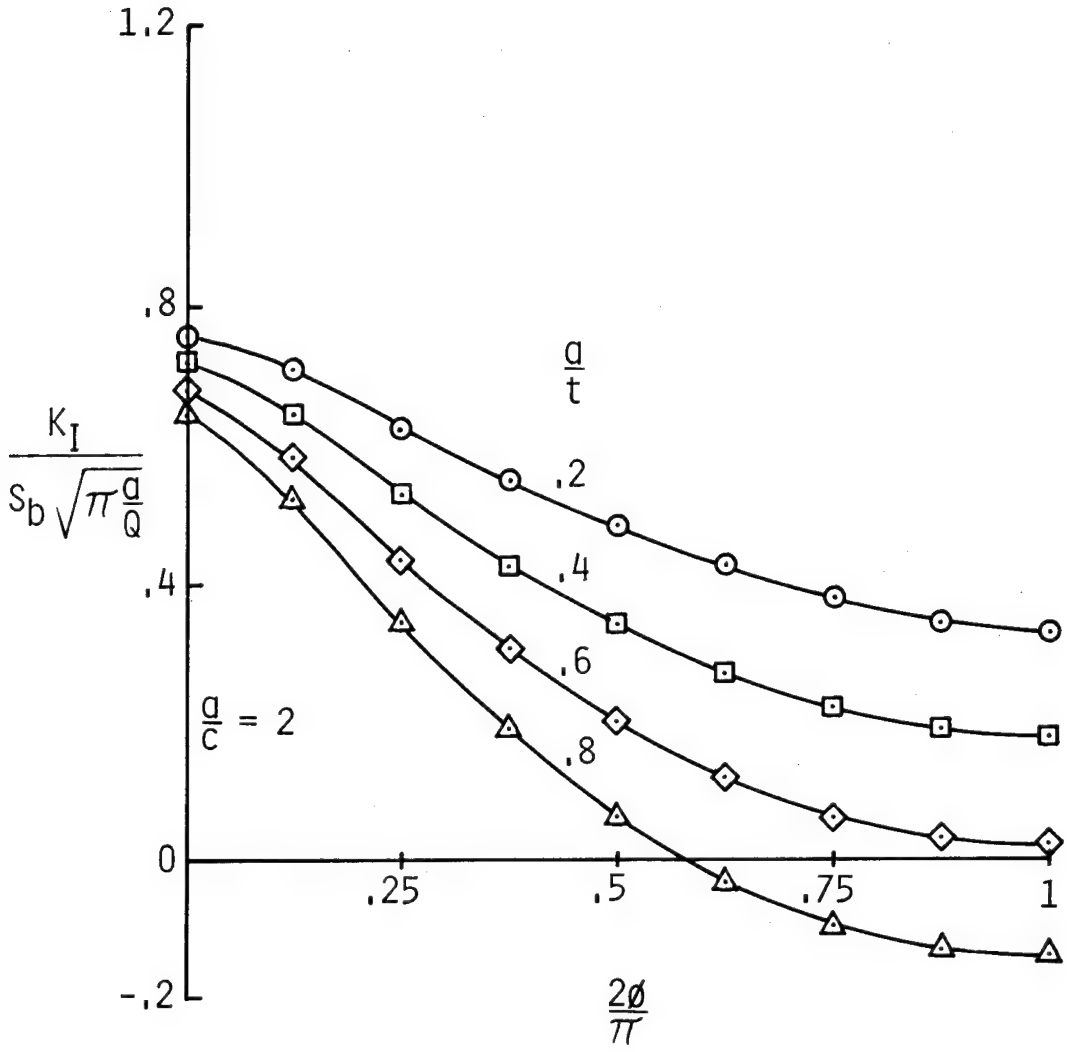

Figure 7.- Concluded.

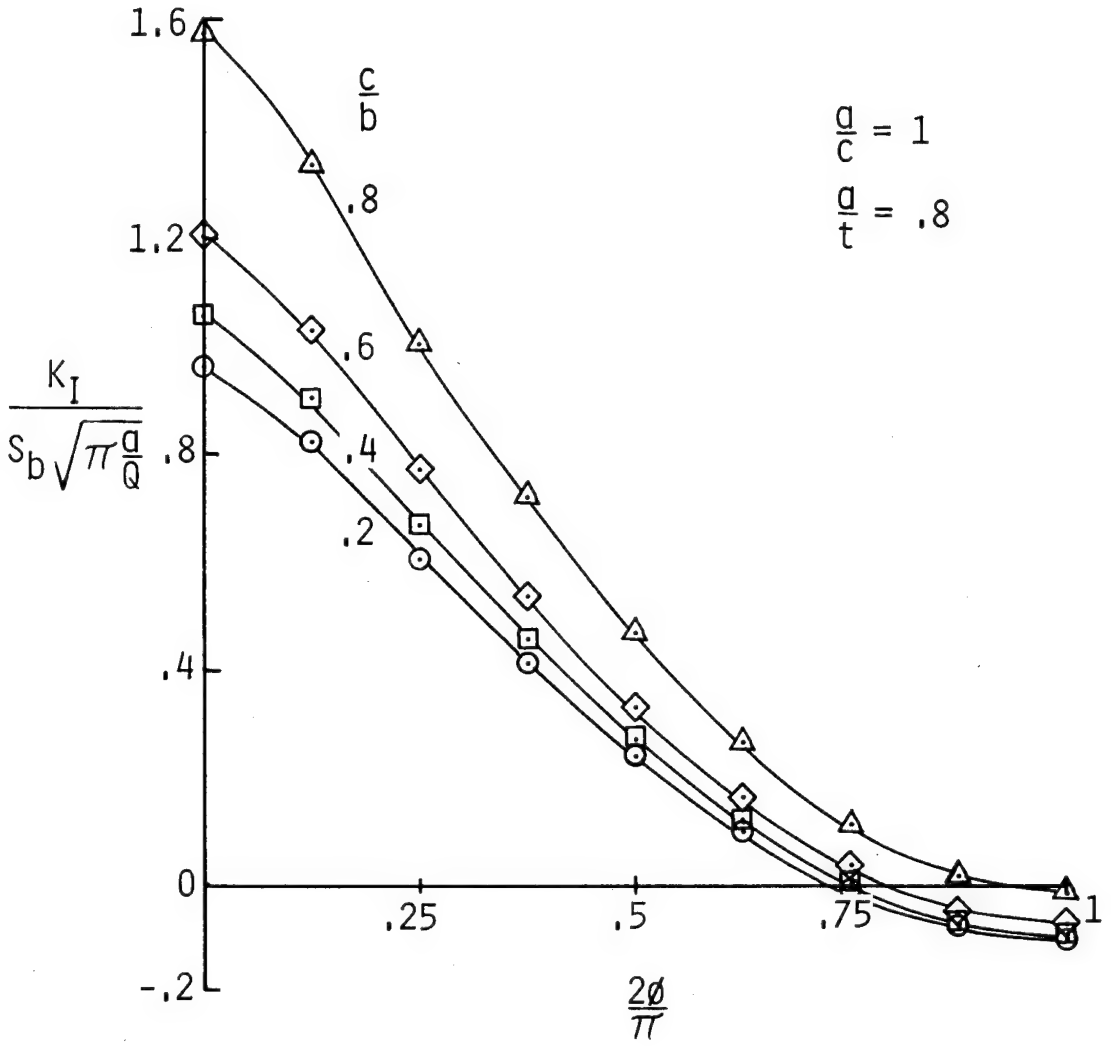

(a) Semicircular crack.

Figure 8.- Normalized stress-intensity factors along the front of a deep surface crack in a plate under bending.

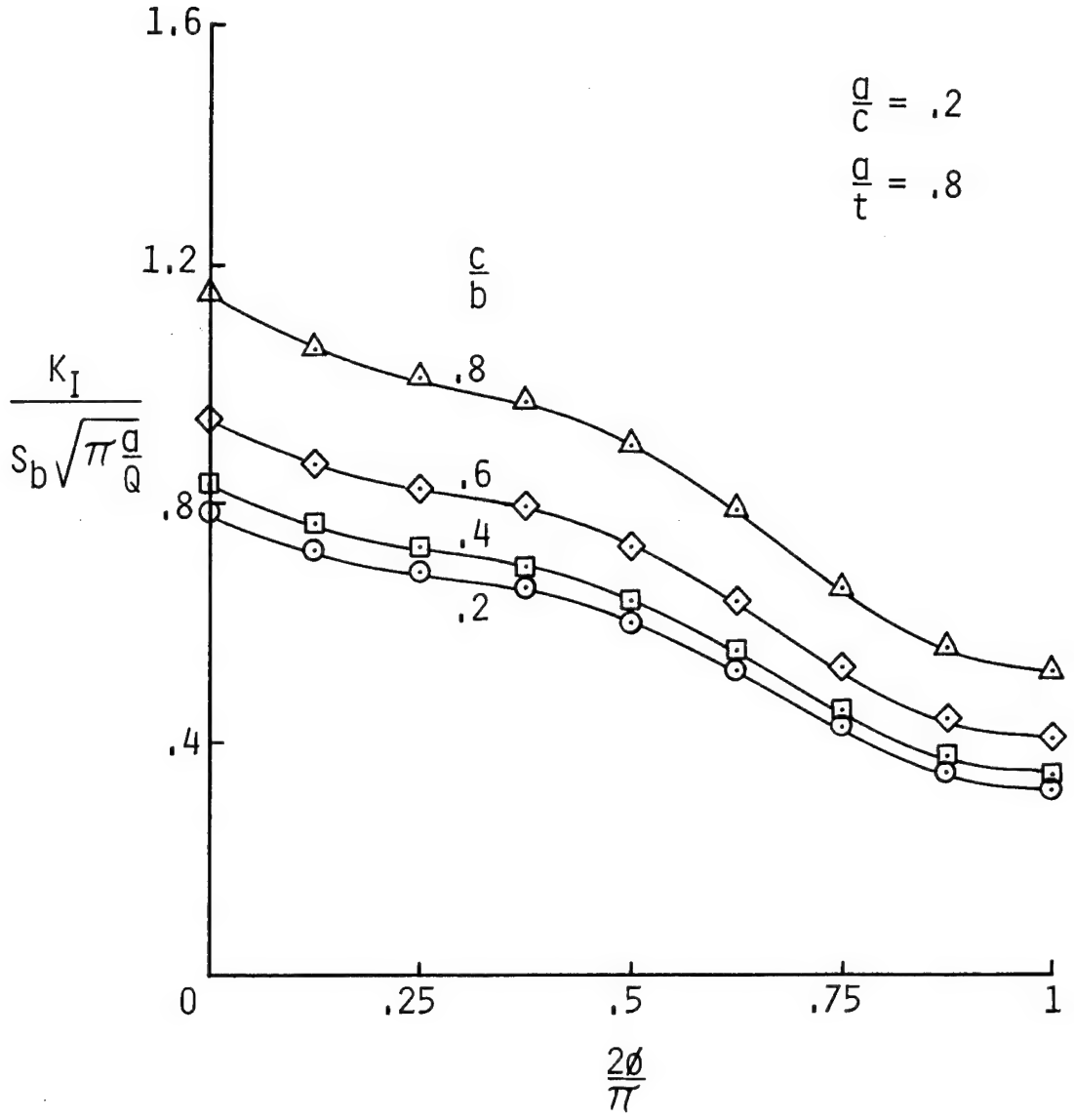

(b) Semielliptical crack.

Figure 8.- Concluded.

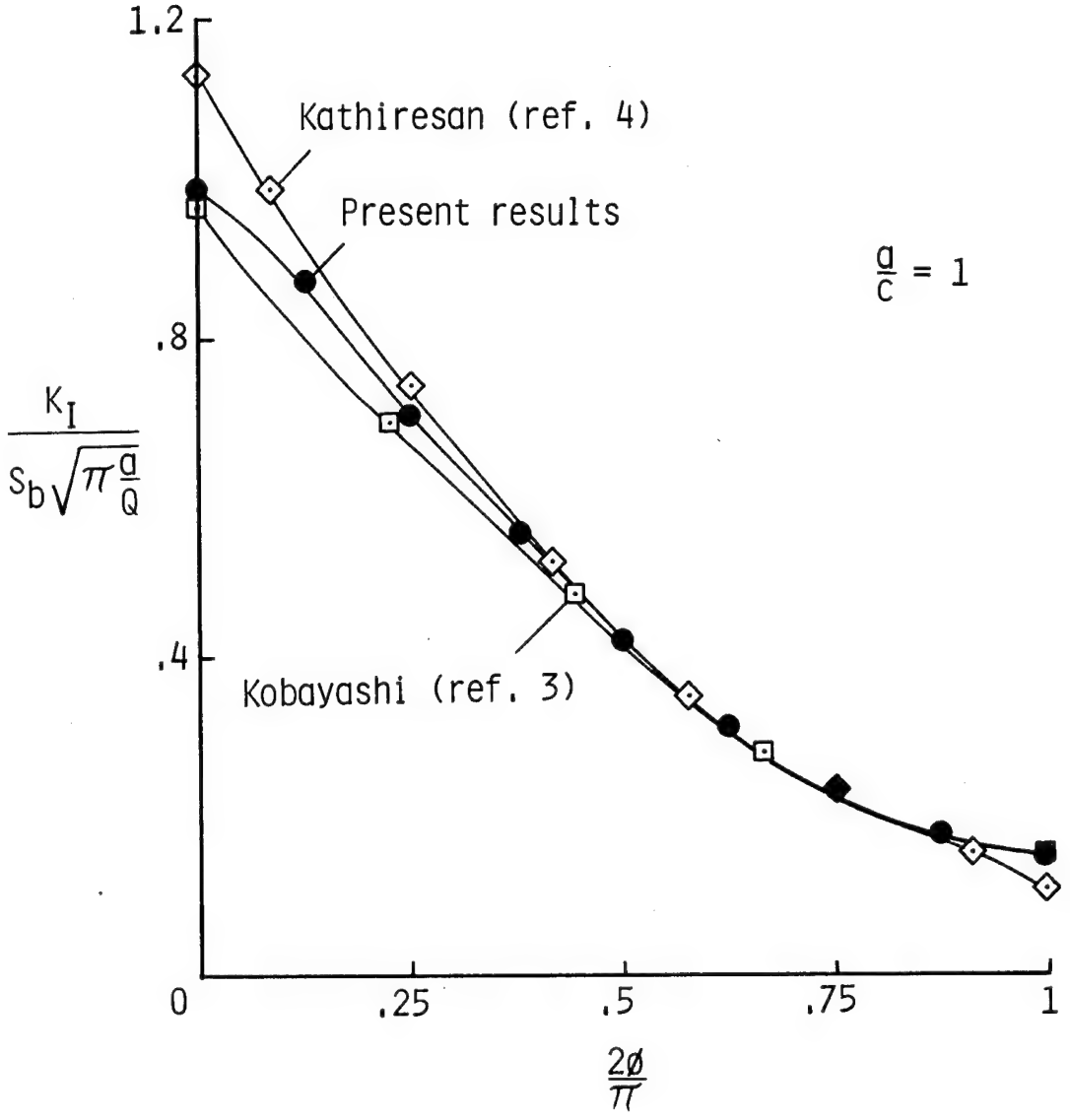

(a) a/t = 0.6.

Figure 9.- Comparison of calculated stress-intensity factors with results from the literature for a semicircular surface crack in a plate under bending.

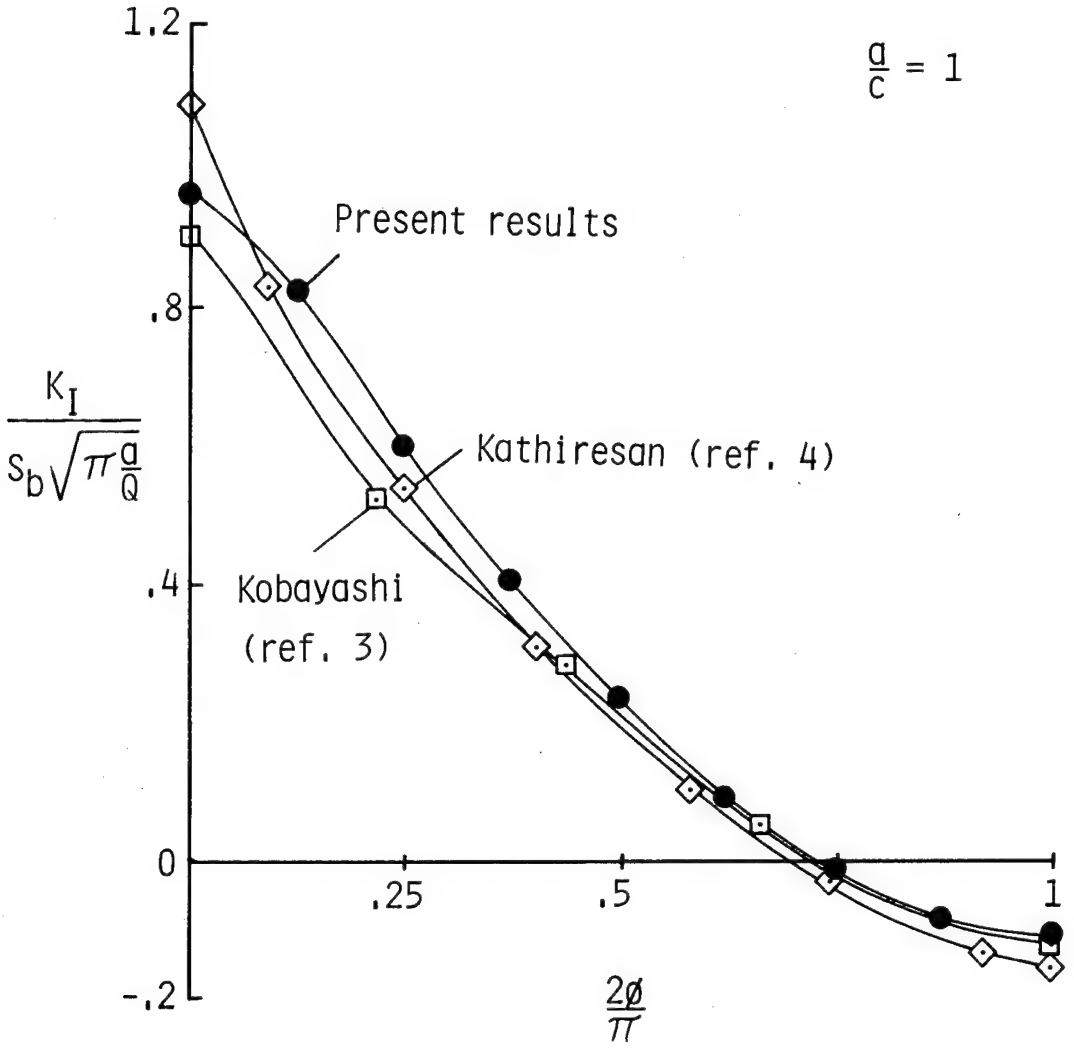

(b) a/t = 0.8.

Figure 9.- Concluded.

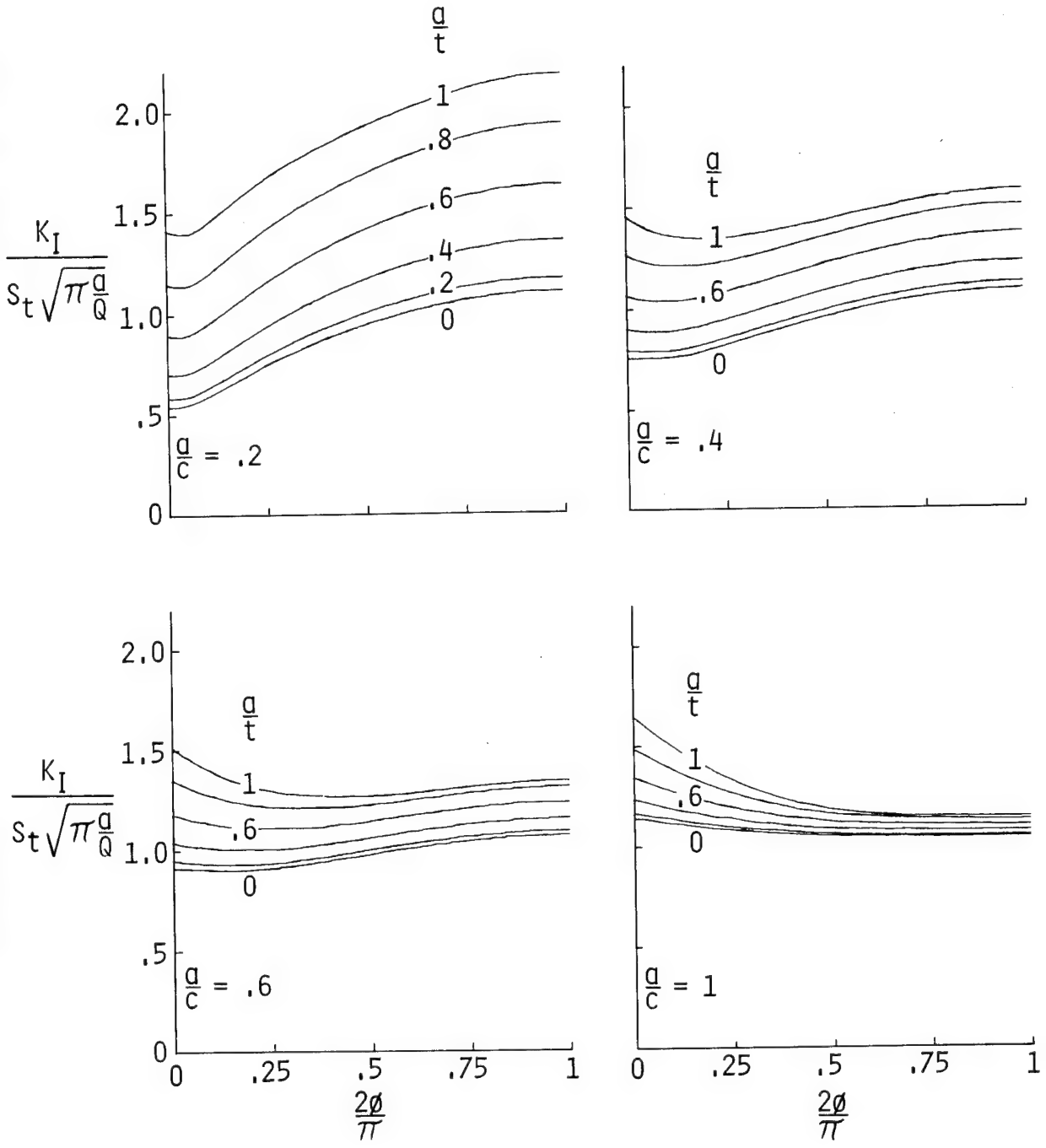

Figure 10.- Typical results from the stress-intensity factor equation (eq. (2)) for a semielliptical surface crack in a plate under tension. (c/b = 0.)

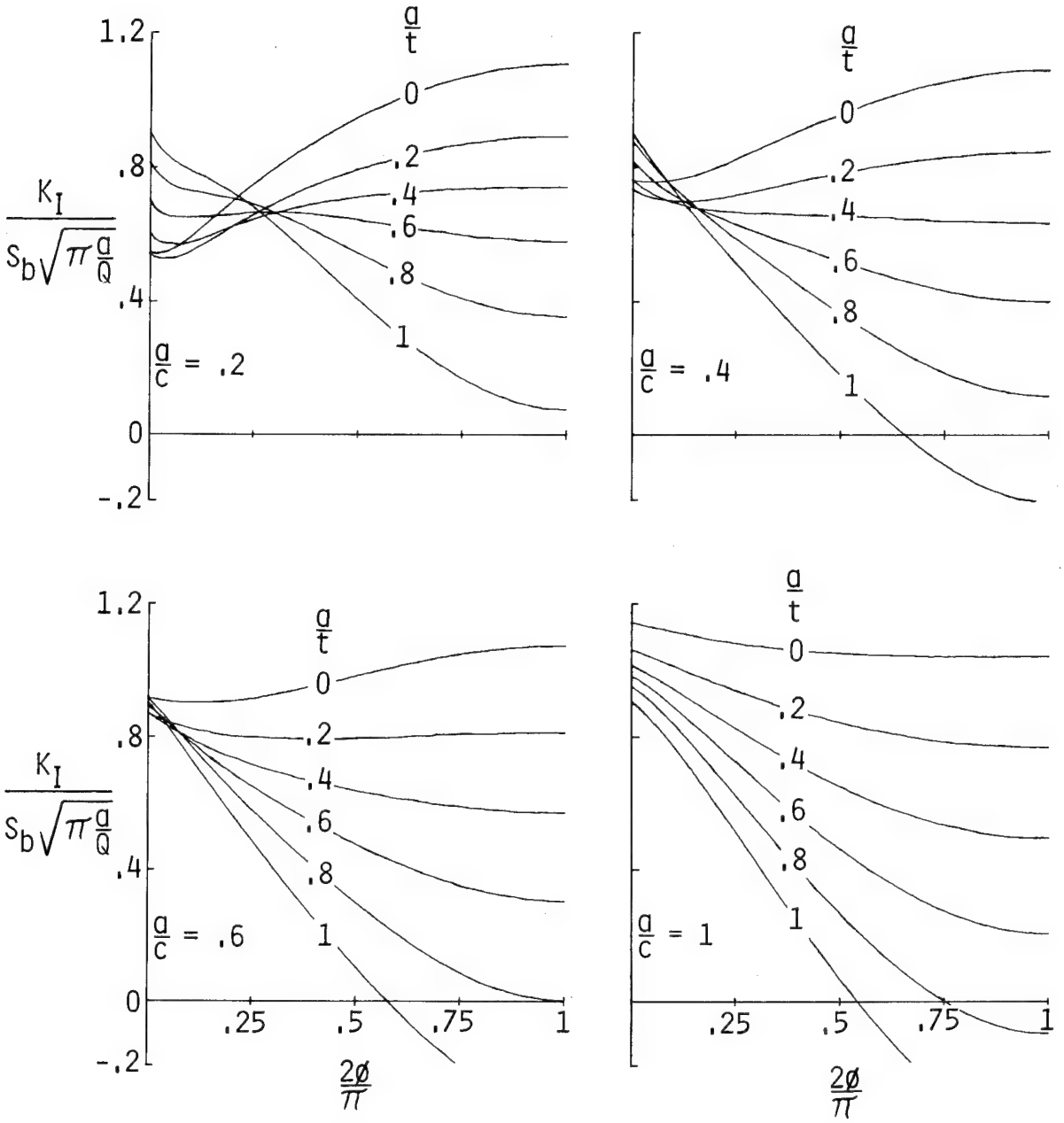

Figure 11.- Typical results from the stress-intensity factor equation (eq. (2)) for a semielliptical surface crack in a plate under bending. (c/b = 0.)

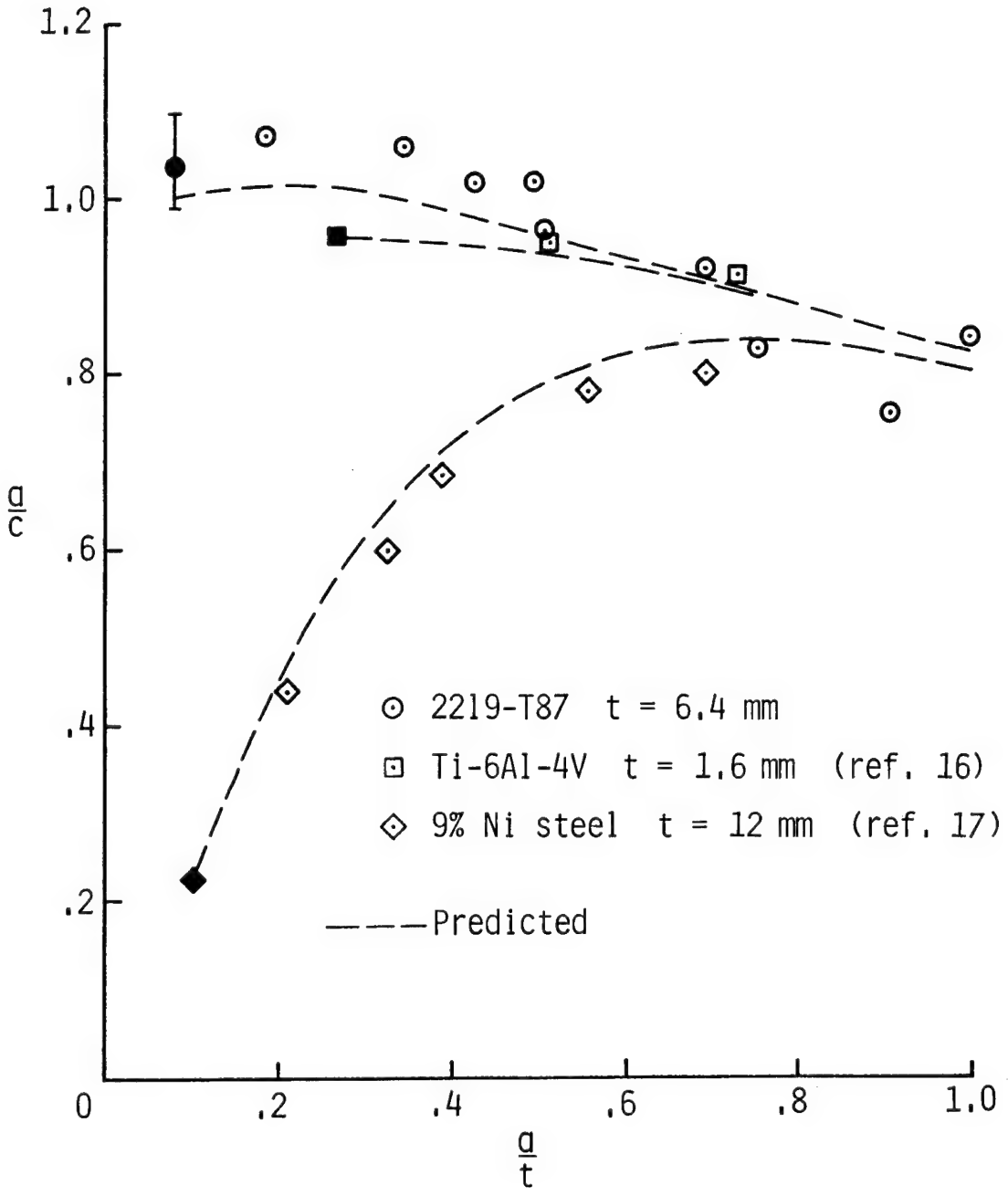

Figure 12.- Experimental and predicted fatigue-crack growth patterns for a surface crack in a plate under tension. (Solid symbols denote initial conditions.)

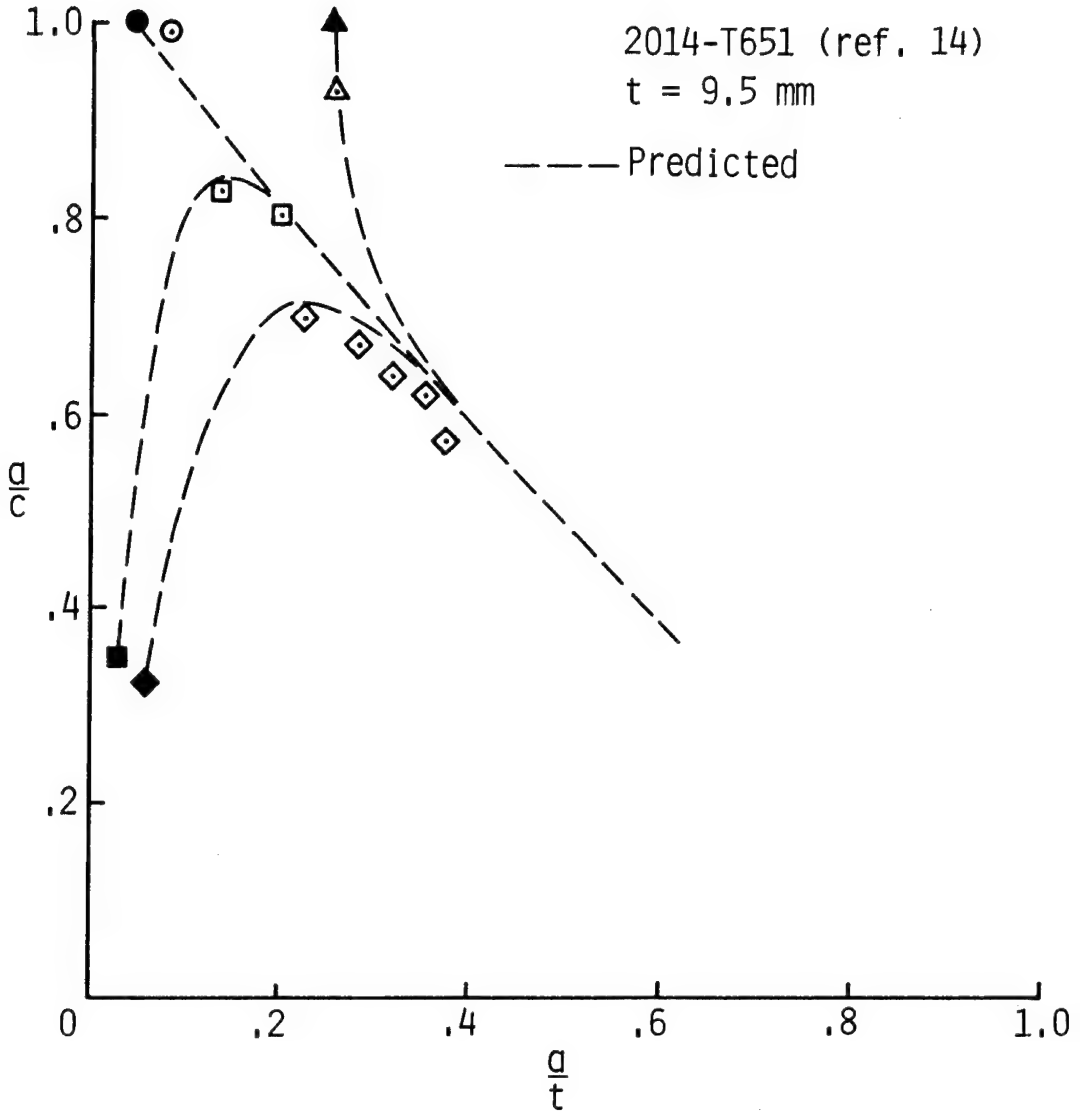

Figure 13.- Experimental and predicted fatigue-crack growth patterns for a surface crack in an aluminum alloy cantilever plate under bending. (Solid symbols denote initial conditions.)

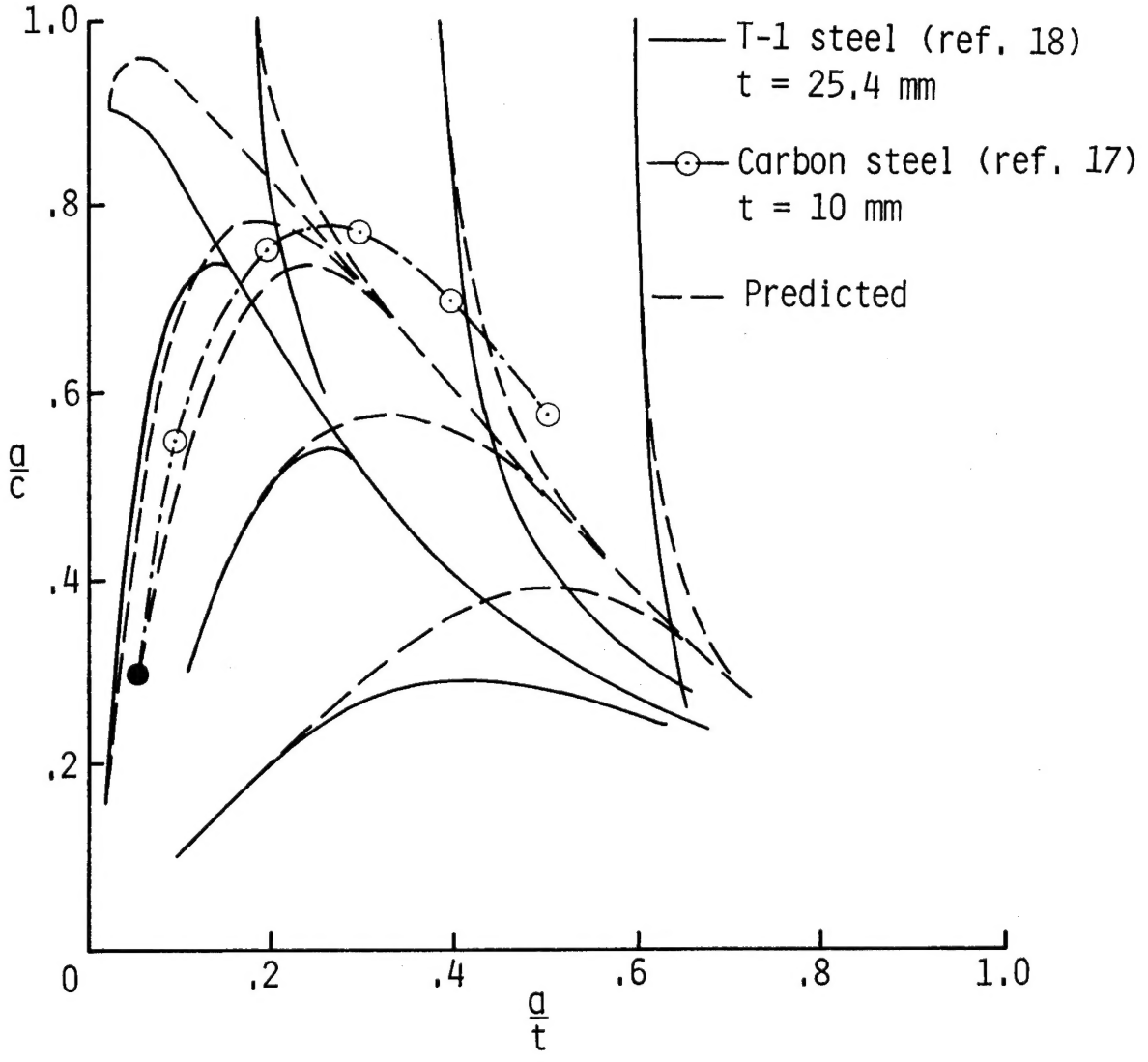

Figure 14.- Experimental and predicted fatigue-crack growth patterns of a surface crack in a steel cantilever plate under bending.

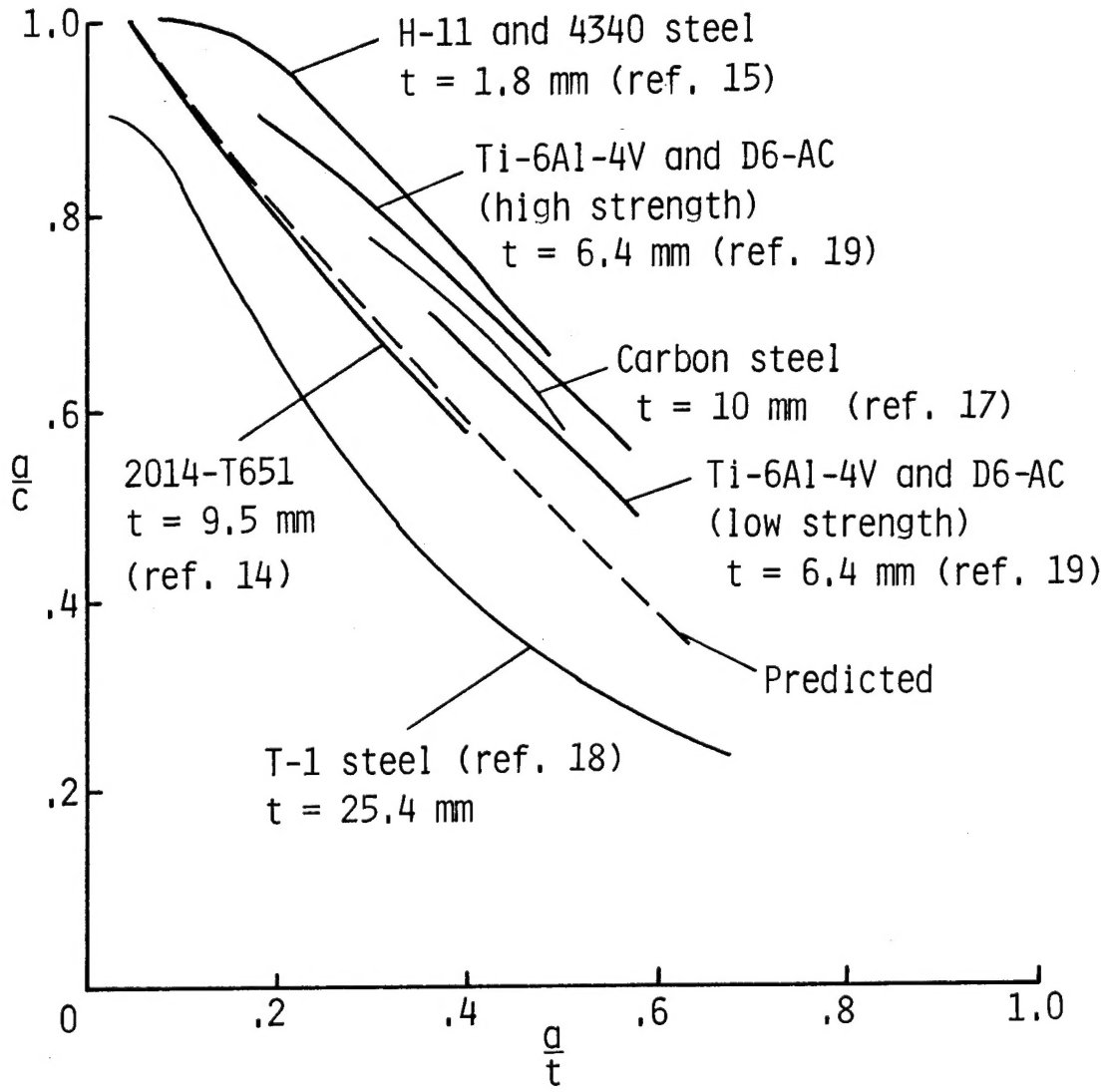

Figure 15.- Experimental and predicted fatigue-crack-growth patterns of surface cracks in plates of various materials under bending.

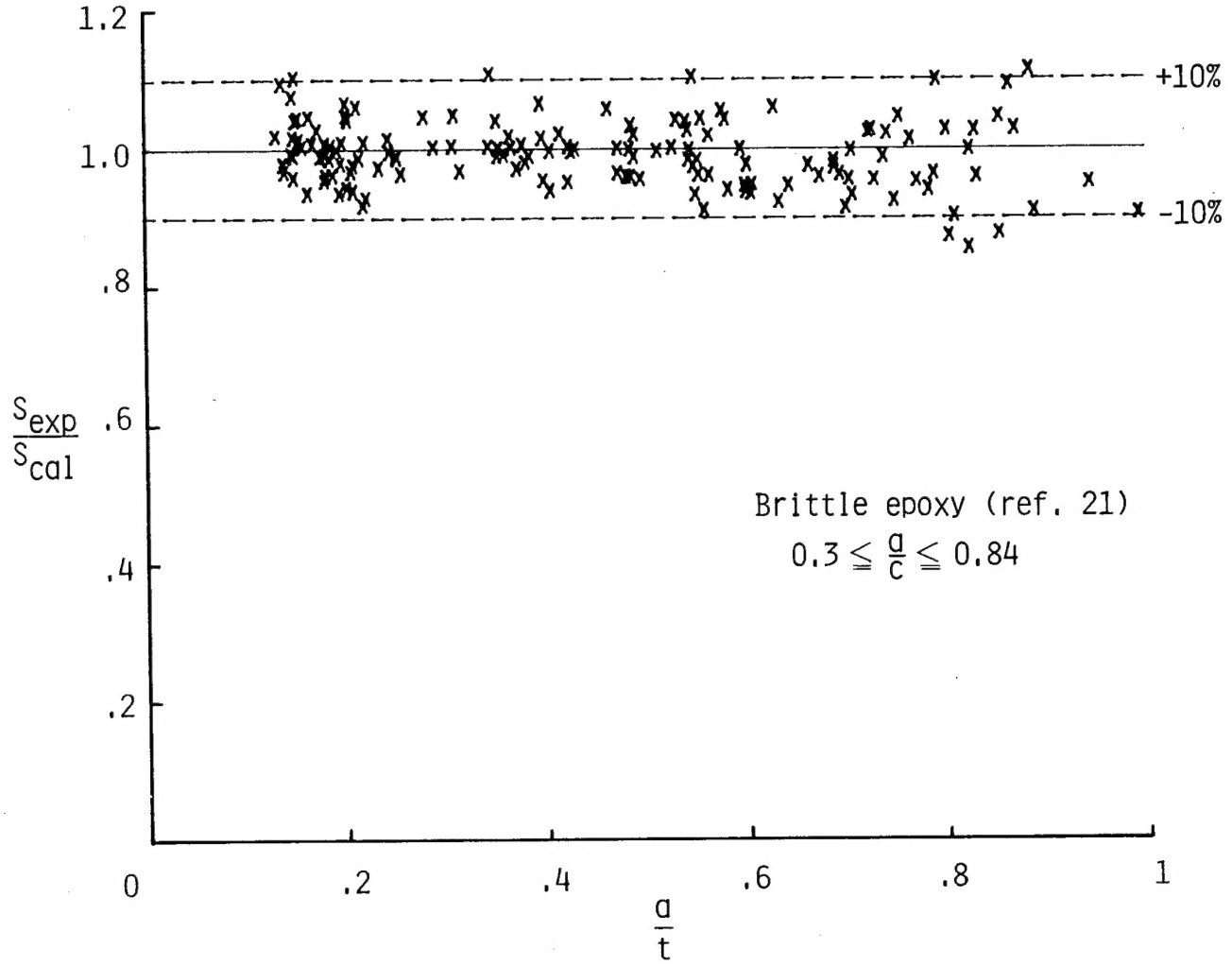

Figure 16.- Correlation of experimental failure stress S_{exp} to calculated failure stress S_{cal} for a brittle epoxy material as a function of a/t.

1. Report No.	2. Government Accession No.	3. Recipient's Catalog No.
NASA TP-1578		

4. Title and Subtitle	5. Report Date
ANALYSES OF SURFACE CRACKS IN FINITE PLATES UNDER TENSION OR BENDING LOADS	December 1979
	6. Performing Organization Code
7. Author(s)	8. Performing Organization Report No.
J. C. Newman, Jr., and I. S. Raju	L-13053
	10. Work Unit No.
9. Performing Organization Name and Address	506-53-53-01
NASA Langley Research Center Hampton, VA 23665	11. Contract or Grant No.
	13. Type of Report and Period Covered
12. Sponsoring Agency Name and Address	Technical Paper
National Aeronautics and Space Administration Washington, DC 20546	14. Sponsoring Agency Code

15. Supplementary Notes

I. S. Raju: The George Washington University, Joint Institute for Advancement of Flight Sciences.

J. C. Newman, Jr.: Langley Research Center.

16. Abstract

This paper presents stress-intensity factors calculated with a three-dimensional, finite-element analysis for shallow and deep semielliptical surface cracks in finite elastic isotropic plates subjected to tension or bending loads. A wide range of configuration parameters was investigated. The ratio of crack depth to plate thickness ranged from 0.2 to 0.8 and the ratio of crack depth to crack length ranged from 0.2 to 2.0. The effects of plate width on stress-intensity variations along the crack front were also investigated.

A wide-range equation for stress-intensity factors along the crack front as a function of crack depth, crack length, plate thickness, and plate width was developed for tension and bending loads. The equation was used to predict patterns of surface-crack growth under tension or bending fatigue loads. A modified form of the equation was also used to correlate surface-crack fracture data for a brittle epoxy material within ±10 percent for a wide range of crack shapes and crack sizes.

17. Key Words (Suggested by Author(s))	18. Distribution Statement
Three-dimensional finite-element analysis Stress-intensity factors Surface cracks	Unclassified - Unlimited Subject Category 39

19. Security Classif. (of this report)	20. Security Classif. (of this page)	21. No. of Pages	22. Price*
Unclassified	Unclassified	43	$4.50

* For sale by the National Technical Information Service, Springfield, Virginia 22161

NASA-Langley, 1979